Research Article

De novo fatty-acid synthesis protects invariant NKT cells from cell death, thereby promoting their homeostasis and pathogenic roles in airway hyperresponsiveness

Jaemoon Koh[1,2,]*, Yeon Duk Woo[2,]*, Hyun Jung Yoo[3], Jun-Pyo Choi[4], Sae Hoon Kim[4,5], Yoon-Seok Chang[4,5], Kyeong Cheon Jung[1], Ji Hyung Kim[3], Yoon Kyung Jeon[1], Hye Young Kim[2], Doo Hyun Chung[1,2]

[1]Department of Pathology, Seoul National University College of Medicine, Seoul, Korea

[2]Laboratory of Immune Regulation in Department of Biomedical Sciences, Seoul National University College of Medicine, Seoul, Korea

[3]Laboratory of Immunology and Vaccine Innovation, Department of Biotechnology, College of Life Sciences and Biotechnology, Korea University, Seoul, Korea

[4]Department of Internal Medicine, Seoul National University Bundang Hospital, Seongnam, Korea

[5]Institute of Allergy and Clinical Immunology, Seoul National University Medical Research Council, Seoul, Korea

Corresponding author:

Doo Hyun Chung

Department of Pathology, Seoul National University College of Medicine,

Laboratory of Immune Regulation, Department of Biosciences, Seoul National University College of Medicine

101 Daehak-ro, Jongno-gu,

Seoul 03080, Korea

Tel: 82-2-740-8915

Fax: 82-2-743-5530

E-mail: doohyun@snu.ac.kr

*J. Koh and Y. D. Woo contributed equally to this work

Abstract

Invariant natural-killer T (*i*NKT) cells play pathogenic roles in allergic asthma in murine models and possibly also humans. While many studies show that the development and functions of innate and adaptive immune cells depend on their metabolic state, the evidence for this in *i*NKT cells is very limited. It is also not clear whether such metabolic regulation of *i*NKT cells could participate in their pathogenic activities in asthma. Here, we showed that acetyl-coA-carboxylase 1 (ACC1)-mediated *de novo* fatty-acid synthesis is required for the survival of *i*NKT cells and their deleterious functions in allergic asthma. ACC1, which is a key fatty-acid synthesis enzyme, was highly expressed by lung *i*NKT cells from WT mice that were developing asthma. *Cd4*-Cre*Acc1*$^{fl/fl}$ mice failed to develop OVA-induced and HDM-induced asthma. Moreover, *i*NKT cell-deficient mice that were reconstituted with ACC1-deficient *i*NKT cells failed to develop asthma, unlike when WT *i*NKT cells were transferred. ACC1 deficiency in *i*NKT cells associated with reduced expression of fatty acid-binding proteins (FABPs) and peroxisome proliferator-activated receptor (PPAR)γ, but increased glycolytic capacity that promoted *i*NKT-cell death. Furthermore, circulating *i*NKT cells from allergic-asthma patients expressed higher *ACC1* and *PPARG* levels than the corresponding cells from non-allergic-asthma patients and healthy individuals. Thus, *de novo* fatty-acid synthesis prevents *i*NKT-cell death *via* an ACC1-FABP-PPARγ axis, which contributes to their homeostasis and their pathogenic roles in allergic asthma.

Introduction

Invariant natural-killer T (*i*NKT) cells are a subset of innate T cells that express a restricted T-cell receptor (TCR) repertoire (Vα24-Jα18 in humans and Vα14-Jα18 in mice) and respond to glycolipids presented on the CD1d molecule. One such glycolipid is α-galactosylceramide (α-GalCer), which originates from a marine sponge and strongly activates *i*NKT cells *in vitro* and *in vivo* [1, 2]. Once activated, *i*NKT cells secrete a diverse array of cytokines, including interferon (IFN)γ, interleukin (IL)-4, IL-13, IL-17A, and IL-10 [3]. These *i*NKT cell-derived cytokines play important roles in the pathogenesis of various immunological diseases, including sepsis, arthritis, tumors, and asthma [4, 5, 6, 7]. With regard to the latter, *i*NKT cells are one of the key effectors that promote allergic asthma in murine models. Specifically, by secreting IL-4, *i*NKT cells stimulate the differentiation of T-helper (Th)2 cells and their responses. Moreover, by secreting IL-13, *i*NKT cells promote the contraction of airway smooth muscle, which is a cardinal feature of asthma [8 9]. In addition, we recently reported that *i*NKT cells contribute to the development of asthma by secreting X-C motif chemokine ligand-1, which recruits conventional X-C motif chemokine receptor 1-expressing type-1 dendritic cells into the lungs: this then stimulates the Th2 responses that drive asthma [10]. Thus, *i*NKT cell-derived soluble factors play multiple critical roles in the development of allergic asthma in murine models. It should be noted that it is somewhat unclear what role *i*NKT cells play in human asthma. Several studies suggest that human asthmatic airways contain large numbers of *i*NKT cells, but this was not observed by other studies [11, 12, 13, 14, 15, 16]. However, a recent review describes additional lines of evidence that suggest that *i*NKT cells do contribute to the development and exacerbation of human asthma development, although the mechanisms may not necessarily involve increased *i*NKT-cell frequencies. Thus, further research on the roles of *i*NKT cells in mouse models and humans with asthma is needed to improve our understanding of the pathogenesis of this disease.

Many studies show that the development and functions of innate and adaptive immune

cells are dependent on the metabolic states of these cells [17]. In particular, the metabolic balance between glycolysis and oxidative phosphorylation (OXPHOS) shapes the differentiation and functions of $CD4^+$ Th cells, $Foxp3^+$ regulatory T cells (Tregs), cytotoxic $CD8^+$ T cells, and macrophages [18]. The development and functions of *i*NKT cells may also depend on their metabolism: while the evidence to date is quite limited [19], the thymic development of *i*NKT cells and their inflammatory cytokine production as mature cells associate with changes in their glycolysis:OXPHOS balance [20]. Moreover, peripheral *i*NKT-cell functions are regulated by their levels of reactive oxygen species, which are byproducts of aerobic metabolism [21]. It is also possible that immune-cell metabolism may participate in asthma since a recent study showed that fatty acid-oxidation inhibitors alleviate house-dust mite (HDM)-induced airway inflammation [22]. Similarly, the airway Th2 cells that mediate allergic responses against HDM depend on glycolysis and lipid metabolism [23].

Several studies show that lipid biogenesis, which is a major metabolic pathway, also affects the differentiation and functions of conventional $CD4^+$ T cells [24, 25, 26]: for example, a CD5-like molecule enforces low cholesterol biosynthesis in Th17 cells, which limits ligand availability for Rorγt, the Th17 master transcription factor, thereby preventing Th17 cells from becoming pathogenic and inducing autoimmunity [23]. Similarly, several studies show that acetyl-CoA-carboxylase 1 (ACC1) affects multiple T-cell subsets. ACC1 is a key fatty-acid synthesis enzyme in the cytosol that catabolizes the ATP-dependent carboxylation of acetyl-CoA to malonyl-CoA [27], and its downregulation impairs the peripheral persistence and homeostatic proliferation of $CD8^+$ T cells, augments Treg development from naïve $CD4^+$ T cells and their suppressive functions, blocks the development of Th17 cells from naïve $CD4^+$ T cells [24, 28], impairs the formation of IL-5-producing $CD4^+$ T cells [29], and promotes $CD4^+$ T-cell development [30]. The T-cell changes caused by inhibiting ACC1 reduce disease severity in murine models of listeria infection, chronic graft-versus-host disease, multiple sclerosis[31], and T cell-mediated asthma [29]; it also promotes resistance to parasites [30]. Thus, by shaping

fatty-acid synthesis, ACC1 can alter pathogenic and protective T-cell responses.

To our knowledge, the role(s) of ACC1-mediated fatty-acid synthesis in other immune cells, including *i*NKT cells, and in asthma have not been assessed. In this study, we used ACC1-deficient (*Cd4*-Cre*Acc1*$^{fl/fl}$) mice and adoptive transfer experiments to determine whether ACC1-mediated fatty-acid metabolism in *i*NKT cells participates in the development of asthma. Indeed, we found that ACC1 promotes the survival of *i*NKT cells by regulating a fatty acid-binding protein (FABP)-PPARγ axis that can downregulate glycolysis. The improved ACC1-mediated *i*NKT-cell survival shapes the homeostasis and functions of these cells, which in turn promote the development of ovalbumin (OVA)- or HDM-induced allergic asthma in mice. We also observed that the ACC1-FABP-PPARγ axis may be active in patients with allergic asthma but not controls.

Results

Activated *i*NKT cells express high levels of a fatty-acid synthesis-related gene whose deletion blocks allergen-induced asthma

To determine whether intracellular metabolic processes in *i*NKT cells play important roles in allergic asthma, *i*NKT cells sorted from the lungs of OVA-induced asthma model mice were assessed for the expression of key enzymes involved in glycolysis, the tricarboxylic acid (TCA) cycle, β-oxidation, and fatty-acid synthesis (Fig. 1). Indeed, OVA challenge significantly increased *i*NKT-cell expression of β-oxidation and fatty-acid synthesis enzymes and tended to elevate TCA-cycle enzyme expression. However, glycolysis-enzyme expression remained low (Fig. 1A, B). The significantly upregulated fatty-acid synthesis enzymes were Acc1, Fasn, and Oxsm: Acc1 and Fasn play a particularly key role in *de novo* fatty-acid synthesis. Notably, when purified murine *i*NKT cells and conventional $CD4^+$ and $CD8^+$ T cells were activated *in vitro* with anti-CD3/CD28, the *i*NKT cells expressed much higher levels of *Acc1* and *Fasn* than the other cells. By contrast, the $CD4^+$ and $CD8^+$ T cells expressed higher levels of TCA cycle (*Sdh2b* and *Idh1a*) and glycolysis (*Hk2* and *Pkm2*) enzymes, respectively (Fig. 1C). This is consistent with the previous Gene Set Enrichment Analysis of Oh et al.: when they compared unstimulated murine *i*NKT and $CD4^+$ T cells to each other, they found that genes involved in the 'lipid, fatty acid and steroid metabolism' pathway were enriched in *i*NKT cells (Fig. S1A) [32]. Thus, *i*NKT cells express *Acc1* and *Fasn* when they are stimulated, including in asthma, whereas conventional $CD4^+$ and $CD8^+$ T cells do not.

We then focused on ACC1. To test whether ACC1-mediated *de novo* fatty-acid synthesis in *i*NKT cells shapes AHR and allergic immune responses, we generated *Cd4*-Cre*Acc1*$^{fl/fl}$ mice: the CD4-positive cells (*i.e.* conventional $CD4^+$ T and *i*NKT cells) in these mice cannot express ACC1. Since conventional $CD4^+$ T cells did not upregulate ACC1 when stimulated *in vitro* or *in vivo* (Fig. 1B, C), the knockout is likely to be physiologically

relevant for *i*NKT cells only. When the *Cd4*-Cre*Acc1*$^{fl/fl}$ and *Acc1*$^{fl/fl}$ control mice were induced to undergo OVA-mediated asthma, we indeed observed that the loss of ACC1 expression attenuated AHR (Fig. 1D) and the total immune-cell numbers in the lung and the bronchoalveolar lavage fluid (BALF) (Fig. S1B). These changes associated with significantly decreased total lymphocyte, neutrophil, eosinophil, and macrophage frequencies in the BALF (Fig. S1C) and lower eosinophil frequencies in the lung (Fig. S1D). The lung CD8$^+$ T-cell and alveolar- and interstitial-macrophage frequencies did not change. Importantly, the total lung CD4$^+$ T-cell population (excluding *i*NKT cells) also did not change significantly (Fig. S1D). By contrast, there was a sharp drop in *i*NKT cells in the lung; this was also associated with a significant increase in PI staining (Fig. 1E). qRT-PCR analysis of the conventional lung CD4$^+$ T-cell population (excluding *i*NKT cells) showed that loss of ACC1 expression associated with lower *Gata3*, *Il4*, *Il5*, and *Il13* expression but similar *Tbx21*, *Rorc*, *Foxp3*, *Ifng*, *Il-17a*, and *Il-10* expression (Fig. S1E, F). Indeed, when the lung *i*NKT cells and conventional CD4$^+$ T cells were separately isolated, both *i*NKT cells and the conventional CD4$^+$ T cells demonstrated dramatically lower *Il4* and *Il13* expression but similar *Ifng* and *Il17a* expression (Fig. 1F and Fig. S1F). Notably, all of these findings were recapitulated when we conducted the same analyses in mice that underwent HDM-induced asthma (Fig. 1G–I and Fig. S1G–K). Thus, the inability of lung *i*NKT cells to express ACC1 induced *i*NKT-cell death during allergen-induced asthmogenesis. This also reduced their expression of *Gata3*, *Il4*, *Il5*, and *Il13* in lung conventional CD4$^+$ T cells: these effects markedly reduced the eosinophilia and AHR. These effects were independent of the inability of conventional lung CD4$^+$ T cells to express ACC1 in the mice.

ACC1-deficient *i*NKT cells cannot generate α-GalCer-mediated AHR and their adoptive transfer into *i*NKT cell-deficient mice cannot restore allergen-induced asthma

The experiments above suggest that *i*NKT cells alone mediate ACC1-mediated

regulation of airway inflammation. To test this further, we challenged *Cd4*-Cre*Acc1*$^{fl/fl}$ and *Acc1*$^{fl/fl}$ mice intranasally with α-GalCer, which has been shown previously to induce *i*NKT cell activation-mediated AHR [33]. Consistent with the results from OVA- and HDM-induced asthma models, the *Cd4*-Cre*Acc1*$^{fl/fl}$ mice showed the following: less AHR and lung and BALF inflammation; significantly fewer lymphocytes, neutrophils, and macrophages in the BALF; less eosinophilia in the BALF and lungs; no difference in lung CD4$^+$ and CD8$^+$ T-cell frequencies but significantly fewer lung *i*NKT cells and greater PI staining of these cells; lower expression by the lung conventional CD4$^+$ T-cell population of *Gata3, Il4, Il5,* and *Il13* but not *Tbx21, Rorc, Foxp3, Ifng, IL17a, or Il10*; and similar *Ifng* and *Il17a* expression but dramatically reduced *Il4* and *Il13* expression by the lung *i*NKT cells (Fig. 2A–H). Thus, ACC1-deficient *i*NKT cells also failed to promote α-GalCer-induced AHR.

To further confirm that it is the ACC1 in *i*NKT cells that regulated AHR, we adoptively transferred WT *i*NKT cells (*i.e.* from *Acc1*$^{fl/fl}$ mice) or ACC1-deficient *i*NKT cells into Jα18 KO mice, which lack NKT cells [34]. The mice were then subjected to OVA-induced asthma. The WT *i*NKT cells, but not the ACC1-deficient *i*NKT cells, restored the following features: AHR (Fig. 3A); the high total immune-cell numbers in the BALF and lungs (Fig. 3B); the high lymphocyte, neutrophil, eosinophil, and macrophage frequencies in the BALF and lungs (Fig. 3C, D); the high *Gata3, Il4, Il5,* and *Il13* expression by the lung CD4$^+$ T-cell population (Fig. 3E, F). As expected, neither adoptively transferred cell type affected the *Tbx21, Rorc, Foxp3, Ifng, Il17a,* and *Il10* expression by the lung conventional CD4$^+$ T-cell population (Fig. 3E, F). Moreover, the transfer of WT *i*NKT cells restored the *i*NKT cell-numbers in the lungs and their expression of *Il4* and *Il13* without changing their *Ifng* and *Il17a* expression; by contrast, transfer of ACC1-deficient *i*NKT cells led to very low *i*NKT-cell frequencies in the lung and low expression of all cytokines (Fig. 3G, H). In addition, the adoptively transferred ACC1-deficient *i*NKT cells in the lung displayed more apoptosis than the transferred WT *i*NKT cells (Fig. 3I). Lastly, transfer of the WT *i*NKT cells associated with significantly

higher histological lung scores than transfer of the ACC1-deficient *i*NKT cells (Fig. 3J). Thus, ACC1-deficient *i*NKT cells cannot promote AHR in allergic asthma models.

ACC1-deficient *i*NKT cells exhibit defects in thymic development, homeostasis, and activation

To investigate the effects of ACC1-mediated metabolic programming on the development and function of *i*NKT cells, we examined the thymic development and peripheral homeostasis of *i*NKT cells in *Cd4*-Cre*Acc1*$^{fl/fl}$ mice. Mature *Cd4-Acc1*$^{fl/fl}$ mice had fewer *i*NKT cells in the thymus, spleen, and liver than *Acc1*$^{fl/fl}$ mice (Fig. S2A). By contrast, the conventional CD4^{+} and CD8^{+} T-cell numbers in the thymus and spleen were not affected by *Cd4-Acc1*$^{fl/fl}$ (Fig. S2B). However, the ACC1 deletion did not alter the frequencies of the NKT1, NKT2, and NKT17 subsets in the *i*NKT-cell population at any of the developmental stages, namely, stage S1 (CD24^{+}c-Kit^{-}CD44^{-}), stage S2 (CD24^{+}c-Kit^{-}CD44^{+}), and stage S3 (CD24^{+}c-Kit^{+}CD44^{+}) (Fig. S2C). Thus, ACC1 deficiency appeared to reduce *i*NKT-cell numbers.

This was tested further by generating mixed bone marrow (BM) chimera mice: thus, a 1:1 ratio of CD45.1^{+} WT BM cells and CD45.2^{+} *Cd4-Acc1*$^{fl/fl}$ BM cells were transferred into lethally irradiated CD45.2^{+} WT recipient mice (Fig. S2D). The ACC1-deficient BM cells generated markedly fewer *i*NKT cells in the thymus, spleen, and liver than the WT BM cells (Fig. S2E, F). This confirmed that ACC1 deficiency induced an intrinsic defect in *i*NKT-cell thymic development and peripheral homeostasis. Moreover, when *i*NKT cells sorted from the livers of *Cd4-Acc1*$^{fl/fl}$ and *Acc1*$^{fl/fl}$ mice underwent TCR ligation with anti-CD3/CD28 *in vitro*, the ACC1-deficient cells produced less CD69 activation marker and cytokine (Fig. S2G, H).

Thus, ACC1 plays a cell-intrinsic role in the regulation of *i*NKT-cell thymic development, peripheral homeostasis, and activation.

Enhanced glycolysis promotes the cell death of ACC1-deficient *i*NKT cells

To investigate the mechanism(s) by which ACC1-mediated metabolic programming of *i*NKT cells promotes allergic asthma, we subjected the sorted unstimulated *i*NKT cells from *Cd4*-Cre*Acc1*$^{fl/fl}$ and *Acc1*$^{fl/fl}$ mice to transcriptome and metabolome analyses (Fig. 4A–D). The ACC1-deficient *i*NKT cells displayed distinct metabolic reprogramming compared to WT *i*NKT cells. Specifically, they exhibited low fatty-acid synthesis but high glycolysis. Indeed, compared to WT *i*NKT cells, their extracellular acidification rate (ECAR), glucose uptake, and expression of Glut1 and other glycolysis-related genes were higher while their expression of gluconeogenesis genes were lower. However, their oxygen consumption rate (OCR) was similar (Fig. 4E–H). Furthermore, the transcriptome analysis revealed significantly altered levels of cell death-related genes in ACC1-deficient *i*NKT cells (Fig. 4C). These observations suggest that ACC1-deficient *i*NKT cells are prone to dying and that this may correlate positively with glycolysis. Indeed, the ECAR and cell death in ACC1-deficient *i*NKT cells correlated positively (Fig. 4I). This relationship was confirmed by treating the ACC1-deficient *i*NKT cells with 2-deoxy-D-glucose (2-DG), which inhibits glycolysis [35]: this decreased their cell death and expression of the pro-apoptotic genes while increasing their expression levels of anti-apoptotic genes. These effects were not observed in WT *i*NKT cells (Fig. 4J, K). Thus, the high levels of glycolysis in ACC1-deficient *i*NKT cells promote their cell death.

ACC1-mediated metabolic programming promotes PPARγ expression and the subsequent survival of *i*NKT cells

To identify the target genes that regulate the metabolic reprogramming and cell death in ACC1-deficient *i*NKT cells, we analyzed the transcription factors in the transcriptome data described above. This showed that sorted unstimulated ACC1-deficient *i*NKT cells expressed *Pparg* at significantly lower levels than WT *i*NKT cells (Fig. 5A, B). This was also observed

when the cells were stimulated with anti-CD3/CD28: the treatment elevated *Pparg* expression in both cell types but much less in the ACC1-deficient cells (Fig. 5B). Thus, PPAR-γ may play a critical role in ACC1-mediated modification of *i*NKT-cell functions. This is consistent with the fact that PPAR-γ is important for activating genes involved in lipid biosynthesis and the maintenance of metabolic homeostasis [36, 37]. Indeed, when anti-CD3/CD28-stimulated ACC1-deficient *i*NKT cells were treated with the PPARγ agonist pioglitazone, their expression of *Pparg* was not only significantly restored, their expression of the gluconeogenesis genes *Cebpa*, *Fbp1*, and *G6pase* rose while their 2-NBDG uptake, expression of Glut1 and the glycolysis genes *Hk2* and *Pkm2*, and cell death dropped (Fig. 5B–D).

ACC1 catalyzes the carboxylation of acetyl-CoA to malonyl-CoA, which is then converted to the long-chain fatty acid palmitate [38]. We found that treatment with palmitate had similar effects on CD3/CD28-stimulated ACC1-deficient *i*NKT cells as pioglitazone, namely, it increased *Pparg* and gluconeogenesis gene expression and downregulated glycolysis (Fig. 5E). These effects were also observed when unstimulated ACC1-deficient *i*NKT cells were treated with palmitate: *Pparg* expression rose (Fig. 5G) while glucose uptake and cell death dropped (Fig. 5H). Thus, restoring the levels of palmitate, the downstream product of ACC1 activity, restored PPARγ expression, which in turn downregulated glycolysis and thereby protected the cells from cell death.

PPARγ activity can be regulated by a variety of ligands, including fatty acids, whose transport to the nucleus is actively facilitated by fatty acid-binding proteins (FABPs) [39, 40, 41]. The unstimulated ACC1-deficient *i*NKT cells showed depressed expression of the genes encoding FABP1, FABP3, and FABP5 (Fig. 5F). Thus, ACC1 deficiency downregulated the expression of these genes. We then asked whether circumventing the ACC1 deficiency by treating the unstimulated cells with palmitate could improve the expression of these FABPs, as exogenous treatment of palmitate has been shown to induce FABPs in macrophages:

indeed, *Fabp1*, *Fabp3*, and especially *Fabp5* expression were upregulated in *i*NKT cells as well (Fig. 5F).

We then determined whether the FABPs mediate the proglycolytic and pro-apoptotic effects of ACC1 (and palmitate) deficiency in *i*NKT cells by culturing unstimulated palmitate-treated ACC1-deficient *i*NKT cells with a FABP inhibitor, FABP-IN-1, which is known to inhibit FABP 3, 5 and 7. Indeed, the inhibitor blocked the ability of palmitate to restore PPARγ expression (Fig. 5G) and suppress glucose uptake and cell death (Fig. 5H). These findings were also observed when CD3/CD28-stimulated ACC1-deficient *i*NKT cells were treated with palmitate with and without FABP inhibitor: the FABP inhibitor reversed the ability of palmitate to increase *Pparg* and gluconeogenesis gene expression and downregulate glycolysis (Fig. 5E).

Since FABP-inhibitor treatment did not affect the PPARγ expression, glucose uptake, and cell death in WT *i*NKT cells (Fig. 5E, G, H), it seems that the ACC1 deficiency in *i*NKT cells mediated their metabolic reprogramming by abolishing palmitate production: this downregulated their FABP expression, which in turn suppressed PPARγ expression, which increased glycolysis and thereby promoted cell death (Fig. 5I).

On a side note, the WT and ACC1-deficient *i*NKT cells did not differ in terms of the methylation of the promoter site of PPARγ (Fig. S3A), and treatment of the unstimulated cells with histone deacetylase (HDAC) inhibitor did not alter their cell-death rates or expression of *Pparg*, *Hk2*, *Bcl2*, or *Bak* (Fig. S3B, C). Thus, the regulation of PPARγ expression in ACC1-deficient *i*NKT cells may not involve epigenetic changes such as methylation and acetylation.

The ACC1-PPAR-γ axis in *i*NKT cells contributes to AHR and airway inflammation in allergic asthma

To confirm that ACC1-mediated metabolic programming in *i*NKT cells regulates the

development of AHR, we pretreated WT or ACC1-deficient *i*NKT cells with palmitate or pioglitazone, adoptively transferred them into Jα18 KO mice, and then subjected the mice to OVA-induced asthma (Fig. 6) or HDM-induced asthma (Fig. S4). As shown above (Fig. 3), transfer of untreated WT *i*NKT cells was able restore AHR, airway inflammation scores, and high lymphocyte, neutrophil, eosinophil, and macrophage frequencies in the lungs and BALF. It also generated a $CD4^+$ T-cell population in the lungs that expressed high levels of *Gata3*, *Il4*, *Il5*, and *Il13* and low levels of *Tbx21*, *Rorc*, *Foxp3*, *Ifng*, *Il17a*, and *Il10*. Moreover, the sorted *i*NKT cells cells in the lungs expressed high levels of *Il4* and *Il13* but low levels of *Ifng* and *Il17a*. By contrast, transfer of the untreated ACC1-deficient *i*NKT cells did not achieve any of these pathological changes or lung $CD4^+$ T-cell or *i*NKT-cell gene-expression profiles. However, when the ACC1-deficient *i*NKT cells were pretreated with palmitate or pioglitazone, all pathological and gene-expression changes were restored (Fig. 6A–G and Fig. S4).

As shown above (Fig. 3I), the transfer of untreated WT *i*NKT cells into mice that were then subjected to OVA-induced asthma led to a moderate *i*NKT-cell population in the lungs that showed low apoptosis. By contrast, the transfer of untreated ACC1-deficient *i*NKT cells led to low lung *i*NKT cell numbers that frequently took up PI. However, pretreatment of the ACC1-deficient *i*NKT cells with palmitate or pioglitazone increased lung *i*NKT-cell numbers and reduced their apoptosis (Fig. 6H, I). This is consistent with our *in vitro* experiments with the unstimulated and anti-CD3/CD28-stimulated *i*NKT cells above (Fig. 5). Notably, the sorted *i*NKT-cell population in the lungs of Jα18 KO mice that received untreated ACC1-deficient *i*NKT cells also demonstrated less PPARγ expression and more glucose uptake and Glut1 expression compared to when untreated WT *i*NKT cells were transferred, and this was reversed when the ACC1-deficient *i*NKT cells were pretreated with palmitate or pioglitazone (Fig. 6J). Thus, treatment with palmitate or pioglitazone increased the survival of adoptively transferred ACC1-deficient *i*NKT cells in Jα18 KO mice, which restored their ability to

induce AHR in allergic asthma.

Altogether, these results show that ACC1-mediated metabolic programming in *i*NKT cells maintains their PPARγ expression, which downregulates their glycolysis and thereby increases their survival. This allows these cells to promote AHR and airway inflammation in allergic asthma models.

The ACC1-PPARγ axis in *i*NKT cells may also contribute to allergic asthma in humans

We next asked whether patients with allergic asthma demonstrate altered expression of fatty-acid synthesis-related metabolic enzymes in *i*NKT cells compared to healthy volunteers. Thus, we sorted the *i*NKT, Treg, $CD4^+$ T, and $CD8^+$ T cells from the PBMCs of 10 healthy volunteers, 10 patients with allergic asthma, and 10 patients with nonallergic asthma and examined their mRNA expression of *ACC1* and *PPARG*. We also examined the expression of *FASN* because it, like ACC1, is a key *de novo* fatty-acid synthesis enzyme and our experiment with CD3/CD28-stimulated murine *i*NKT cells and conventional $CD4^+$ and $CD8^+$ T cells showed that the *i*NKT cells expressed much higher levels of *Fasn* as well as *Acc1* than the other cells (Fig. 1C). Indeed, circulating *i*NKT cells from allergic asthma patients expressed significantly higher levels of *ACC1*, *FASN*, and *PPARG* than *i*NKT cells from healthy controls and nonallergic asthma patients (Fig. S5A). Similarly, the *i*NKT cells from the allergic asthma patients expressed significantly higher *FBP1* levels than the control *i*NKT cells, although this difference was not observed for *HK2* (Fig. S5B). These changes in *ACC1*, *FASN*, *PPARG*, and *FBP1* expression were much more pronounced in the *i*NKT cells from allergic asthma patients than in the $CD4^+$ T cells, $CD8^+$ T cells, and Tregs from the same patients (Fig. S5). Thus, *i*NKT cells from allergic asthma patients express higher *ACC1*, *FASN* and *PPARG* levels and lower levels of a glycolysis gene than *i*NKT cells from healthy controls and nonallergic asthma patients. These findings suggest that the ACC1-PPAR-γ axis in *i*NKT cells may also be involved in human allergic asthma.

Discussion

The present study showed that *Cd4*-Cre*Acc1*$^{fl/fl}$ mice exhibited attenuated AHR and airway inflammation in OVA- and HDM-induced asthma models due to the enhanced apoptosis and loss of *Gata3*, *Il4*, and *Il13* expression in lung *i*NKT cells. The mechanism appeared to partly involve the low production in *i*NKT cells of the ACC1-downstream long-chain fatty acid palmitate, which impaired FABP expression; this reduced PPARγ expression and enhanced glycolysis in the *i*NKT cells, which promoted their apoptosis. Moreover, the *Cd4*-Cre*Acc1*$^{fl/fl}$ mice displayed significant defects in the thymic development and peripheral homeostasis of *i*NKT cells in a cell-intrinsic manner; thus, homeostatic dysregulation of *i*NKT cells may also contribute to the attenuation of AHR in *Cd4*-Cre*Acc1*$^{fl/fl}$ mice.

The negative effect of ACC1 deficiency on the asthmogenic *i*NKT-cell functions is consistent with several studies that suggest that ACC1-mediated *de novo* fatty-acid synthesis can also shape the behavior of other T cells, including Th17-cell and Treg differentiation, IL-5 production by Th2 cells in the lungs, the generation of memory CD4$^+$ T cells, and CD8$^+$ T-cell proliferation. Like us, these studies also show that blocking ACC1 function can improve various diseases in mouse models [24, 29, 30, 42].

It should be noted that *Cd4*-Cre*Acc1*$^{fl/fl}$ mice lack ACC1 expression in both conventional CD4$^+$ T cells and *i*NKT cells. However, several of our experiments suggest that the amelioration of asthma in *Cd4*-Cre*Acc1*$^{fl/fl}$ mice largely reflects the ACC1 deficiency in *i*NKT cells rather than in other CD4$^+$ T-cell subsets, as follows: (i) *in vitro* TCR ligation upregulated ACC1 expression in *i*NKT cells but not CD4$^+$ T cells; (ii) *in vitro* TCR ligation also upregulated *Fasn*, another *de novo* fatty-acid synthesis gene, in *i*NKT cells but not CD4$^+$ T cells; (iii) the OVA/HDM-challenged ACC1-deficient mice demonstrated a significant reduction in lung *i*NKT-cell numbers but not lung CD4$^+$ T-cell numbers; (iv) the *i*NKT cells, but not CD4$^+$ T cells, in the lung of OVA/HDM-challenged ACC1-deficient mice displayed downregulation of *Gata3*, *Il4*, and *Il13*, which excludes the possibility that ACC1 deficiency

in Th2 cells contributed to the AHR attenuation; (v) the $CD4^+$ T-cell population in the OVA/HDM-challenged lung of the ACC1-deficient mice did not demonstrate downregulation of the Treg markers *Foxp3* and *Il10*, the Th17 markers *Rorc* and *Il17a*, or the Th1 marker *Ifng*, which excludes the possibility that ACC1 deficiency in Tregs, Th17, or Th1 cells contributed to the AHR attenuation; and (vi) *i*NKT cell-deficient mice effectively developed OVA-induced asthma when they were reconstituted with WT *i*NKT cells but not when they were reconstituted with ACC1-deficient *i*NKT cells. These findings together indicate that ACC1-mediated *de novo* fatty-acid synthesis in *i*NKT cells promotes AHR in murine asthma.

The possibility that ACC1 regulates the functions of *i*NKT cells by programming their metabolism was first revealed by our transcriptome analysis of treatment-naïve *i*NKT cells: the ACC1-deficient *i*NKT cells exhibited downregulation of fatty-acid synthesis genes, as could be expected, but also upregulation of glycolysis pathway-related genes. This impaired the survival of the cells: compared to the WT *i*NKT cells, the ACC1-deficient *i*NKT cells were prone to apoptosis. This was observed in ACC1-deficient *i*NKT cells regardless of whether they were treatment-naïve, stimulated by TCR ligation *in vitro*, or activated during OVA/HDM-mediated asthma. The apoptotic tendency of the ACC1-deficient *i*NKT cells associated with higher pro-apoptotic-gene expression and low anti-apoptotic-gene expression. Moreover, the apoptotic tendency of these cells was completely reversed by treatment with glycolysis inhibitor *in vitro*. These findings are consistent with those of Kumar *et al.*[21], who reported that the production of lactate by *i*NKT cells when their glycolysis is upregulated promotes their cell death.

Our transcriptome assays of naïve *i*NKT cells showed that of the multiple candidate transcription factors that were examined, only *Pparg* was upregulated in WT *i*NKT cells but not ACC1-deficient *i*NKT cells. This difference was augmented by TCR ligation. This suggested that downregulation of PPARγ could mediate the enhanced glycolysis and apoptosis in ACC1-deficient *i*NKT cells. This was supported by the fact that the PPARγ

agonist pioglitazone largely restored gluconeogenesis and downregulated glycolysis and apoptosis in these cells. These findings are consistent with reports that PPARγ regulates the glycolytic pathway, although heterogeneous effects have been noted [43, 44, 45, 46, 47, 48]. Our study also supports Fu et al., who observed that lipid biosynthesis is increased in *i*NKT cells after activation, and that this is mediated by PPARγ. Specifically, PPARγ acts synergistically with the transcription factor PLZF (which drives the acquisition of T-helper effector functions by innate and innate-like lymphocytes) to activate the *Srebf1* transcription factor [49], which regulates lipid biosynthesis. This induces cholesterol synthesis, which is required for the optimal production of IFNγ by the *i*NKT cells. This PPARγ/PLZ-*Srebf1*-cholesterol pathway was found to contribute to anti-tumor immunity [50]. Previous studies also reported that the PPARγ agonist ciglitazone promotes the TGFβ-dependent conversion of naïve effector T cells into Tregs whereas PPARγ deficiency increases the infiltration of Th17 cells into the central nervous system in experimental autoimmune encephalomyelitis. [51, 52]. Thus, PPARγ can regulate the differentiation of naïve $CD4^+$ T cells into both Th17 or Treg cells, which supports the role of PPARγ in *i*NKT-cell homeostasis and functions. However, further research is needed to determine the mechanisms by which PPARγ regulates the metabolic programming and biological changes in *i*NKT cells.

We also explored how PPARγ expression was downregulated in ACC1-deficient *i*NKT cells. Several studies have reported that PPARγ expression can be regulated by endogenous ligands such as FABPs, as well as by histone methylation and acetylation [53, 54], and that these changes can be regulated by the intracellular lipid levels [55, 56]. Indeed, we observed that (i) ACC1-deficient *i*NKT cells demonstrated low FABP expression, (ii) exogenous fatty acid not only reversed the effects of ACC1 deficiency on glycolysis and apoptosis, it also restored the expression of both FABPs and PPARγ, and (iii) treating ACC1-deficient *i*NKT cells with exogenous palmitate or a PPARγ agonist and then transferring them into *i*NKT cell-deficient mice restored AHR in OVA- or HDM-induced asthma models. Thus, the reduced *de novo*

fatty-acid synthesis in ACC1-deficient *i*NKT cells downregulated the expression of FABPs, which decreased the expression and activity of PPARγ, which in turn promoted glycolysis and apoptosis. This FABP-PPARγ axis was also observed in studies on hepatocytes and adipocytes, which reported that FABPs interact with PPARγ, thereby inducing its transactivation [39, 57]. However, we did not observe that PPARγ promoter methylation was altered in the ACC1-deficient *i*NKT cells. Taken together, our findings indicate that the ACC1-FABP-PPARγ axis drives the proglycolytic metabolic reprogramming in ACC1-deficient *i*NKT cells, thereby downregulating *i*NKT-cell homeostasis, and functions, including *i*NKT cell-mediated AHR in asthma models.

Finally, we showed that the ACC1-FABP-PPARγ axis in *i*NKT cells may also play pathogenic roles in human allergic asthma: *i*NKT cells in the blood of patients with allergic asthma expressed higher levels of *ACC1*, *FASN*, and *PPARG* and lower levels of a glycolytic gene than the *i*NKT cells of nonallergic asthma patients and healthy controls. Moreover, these genes were up/downregulated much more strongly in the *i*NKT cells from allergic asthma patients than in the other T-cell subsets from the same patients. Notably, the differences between allergic asthma patients and the control patients did not reflect lower frequencies of *i*NKT cells in the PBMCs from the allergic asthma patients (data not shown). This is consistent with speculation in the literature that *i*NKT cells participate in human asthma by altering their phenotype rather than their frequencies: for example, although asthma patients and controls do not differ in terms of *i*NKT-cell frequencies in the BALF, the asthma *i*NKT cells express more IL-4 [11, 58]. Thus, the ACC1-FABP-PPARγ axis in *i*NKT cells may be activated and thereby contribute to human allergic asthma pathology.

In conclusion, derangement of the ACC1-FABP-PPAR-γ axis induces glycolysis-related impairment of cell viability in *i*NKT cells, which limits their ability to induce AHR and airway inflammation in murine asthma models. Therefore, *de novo* lipid synthesis in *i*NKT cells may play a critical regulatory role in the development of AHR.

Materials and methods

Mice

Female C57BL/6 (B6) mice were obtained from the Orient Company (Seoul, Korea). *Cd4*-Cre mice were purchased from the Jackson Laboratory (stock no. 017336; The Jackson Laboratory, Bar Harbor, ME, USA). *Acc1*$^{fl/fl}$ mice were originally generated and kindly provided by Dr. Salih J. Wakil of the Baylor College of Medicine (Houston, TX, USA). To generate *Cd4*-Cre*Acc1*$^{fl/fl}$ mice, the *Acc1*$^{fl/fl}$ mice were crossed with *Cd4*-Cre mice. The animals were bred and maintained under specific-pathogen-free conditions at the Biomedical Research Institute of Seoul National University Hospital (Seoul, Korea). All experiments were conducted on mice that were 8–10 weeks old. All animal experiments were approved by the Institutional Animal Care and Use Committee at Seoul National University Hospital (SNUH-IACUC). The animals were maintained in an AAALAC International (#001169)-accredited facility in accordance with the Guide for the Care and Use of Laboratory Animals 8th edition.

Generation of PBMCs from healthy subjects and asthmatic patients

In total, 30 human PBMC samples were obtained from healthy control subjects and patients with nonallergic and allergic asthma. The PBMCs were obtained from 30 mL peripheral blood by using Ficoll-Paque (GE Healthcare, Uppsala, Sweden). The *i*NKT, CD4^{+} T, Foxp3^{+} Tregs, and CD8^{+} T cells in the PBMCs were sorted by FACSAria II (Becton Dickinson, San Jose, CA, USA; purity < 95%). All subjects provided informed written consent to participate in the study. The Institutional Review Board of Seoul National University Bundang Hospital approved the human studies (IRB #: B-1901/517–304).

Preparation and activation of murine T and *i*NKT cells

To determine the mRNA expression, transcriptome, metabolome, ECAR, and OCR of T and

*i*NKT cells, the cells were obtained from mice as follows. $CD4^+$ or $CD8^+$ T cells from the thymi, spleens, lungs, and livers of *Acc1*$^{fl/fl}$ and *Cd4*-Cre*Accl1*$^{fl/fl}$ mice were enriched by FACSAria II (Becton Dickinson). To obtain *i*NKT cells, the mononuclear cells of the livers of *Acc1*$^{fl/fl}$ and *Cd4*-Cre*Accl1*$^{fl/fl}$ mice were isolated by Percoll gradient centrifugation. Thereafter, the *i*NKT cells were isolated by using APC-conjugated α-GalCer/CD1d tetramers-unloaded or loaded with PBS-57 from the tetramer facility of the National Institutes of Health (Bethesda, MD, USA) followed by sorting using FACS (purity < 95%). Alternatively, liver mononuclear cells were labeled with APC-conjugated □-GalCer/CD1d tetramers, bound to anti-APC magnetic beads, and enriched on a MACS separator (Miltenyi Biotec, Auburn, CA, USA; purity 89%). *i*NKT, $CD4^+$ T, and $CD8^+$ T cells were stimulated with plate coated anti-CD3 and CD28 antibodies overnight.

Adoptive transfer of *i*NKT cells in allergic asthma models

*i*NKT cells (6.0×10^5) obtained from the lungs of *Acc1*$^{fl/fl}$ and *Cd4*-Cre*Accl1*$^{fl/fl}$ mice were adoptively transferred into experimental mice *via* the intratracheal route.

Antibodies, reagents, and preparation of fatty acids

The antibodies used in flow cytometry are summarized in Table S1. The PPAR□ agonist pioglitazone (E6910), the histone deacetylase (HDAC) inhibitor MG-132 (474790), 2-deoxy-D-glucose (2-DG, D6134), and palmitic acid (C16:0, P9767) were purchased from Sigma-Aldrich (St. Louis, MO, USA). Briefly, palmitic acid was dissolved in sterile water using a vortex and heated to 70°C for 10 min. Palmitic acid was conjugated to bovine serum albumin (BSA, Biosesang, Seongnam, Korea) in serum-free RPMI containing 5% non-esterified fatty acids (NEFA)-free BSA immediately after dissolving as described previously [59]. The conjugated-palmitic acid was shaken at 140 rpm at 40°C for 1 h before being added to the cells. Serum-free RPMI containing 5% NEFA-free BSA was used as the vehicle control.

Cells were treated with pioglitazone at 10 μM, 2-DG at 10 mM, MG-132 at 5 μM, or palmitate at 100 μM.

Flow-cytometric analysis

Single-cell suspensions were preincubated with mouse anti-Fc receptor antibodies (BD Biosciences, Franklin Lakes, NJ, USA), stained with antibodies for 30 min at 4□, washed twice with 1 × PBS, and analyzed using a BD LSRII flow cytometer (BD Biosciences). For intracellular cytokine staining, cells were stained for surface markers, permeabilized, and then stained for intracellular proteins. Cells were permeabilized and fixed with Intracellular Fixation & Permeabilization Buffer (eBioscience, Waltham, MA, USA), according to the manufacturer's protocols. Data were analyzed with FlowJo software (version 10; TreeStar, Ashland, OR, USA).

Measurement of glucose uptake capacity

To assess the uptake of the fluorescent glucose analog 2-NBDG, cells were incubated for 30 min with 50 μM 2-NBDG (Cambridge Bioscience, Cambridge, UK)-supplemented glucose-free RPMI 1640 or RPMI containing 10% (v/v) FBS supplemented with 12.5 nM MitoTracker Deep Red (Thermo Fisher Scientific, Waltham, MA, USA) for 30 min at 37℃, 5% (v/v) CO_2. The cells were washed with 1 × PBS, fixed with 0.5% (w/w) paraformaldehyde (PFA, Sigma), and then captured on a BD LSR Fortessa flow cytometer (BD Biosciences).

Generation of mixed BM chimeras

BM cells were prepared from the femurs and tibias of WT B6 ($CD45.1^+$ background) or *Cd4-Acc1*$^{fl/fl}$ B6 ($CD45.2^+$ background) donor mice. Recipient mice ($CD45.2^+$ background) were lethally irradiated (800 rads) and injected intravenously with a 1:1 mixture of BM cells from

WT and *Cd4*-Cre*Acc1*$^{fl/fl}$ mice (1 ×10^6 cells) in total. The chimeras were analyzed 8 weeks after BM transplantation.

OVA- and HDM-induced asthma models

To induce the OVA asthma model, OVA antigen (Sigma) was dissolved in saline to a 1 mg/mL concentration. The mice were injected intraperitoneally with 4 mg aluminum hydroxide (Thermo Fisher Scientific) mixed with 100 µL OVA in saline (1 mg/mL solution) on days 0 and 7. On days 14, 15, 16, and 17, the isoflurane-anesthetized mice were challenged with 50 µg OVA (1 mg/mL solution) intranasally. Twenty-four h after the last OVA instillation, the mice were sacrificed to measure the AHR. To induce the HDM asthma model, HDM (B82; Greer) ws dissolved in saline to a final concentration of 1 mg/mL. Isoflurane-anesthetized mice were then treated intranasally on days 1–14 with 25 µg HDM solution and, 96 h after the final intranasal instillation, the AHR and other inflammatory variables were measured.

***In vivo* intranasal inoculation of α-GalCer**

Mice were inoculated intranasally with 200 ng of α-GalCer dissolved in 50 µL PBS and, 24 h after the last instillation, the mice were sacrificed to measure the AHR.

Measurement of AHR

AHR was measured by administering increasing doses of methacholine (0, 5, 10, 20, and 40 mg/mL) using the forced oscillation technique (FlexiVent System; SCIREQ, Montreal, Quebec, Canada). A snapshot perturbation maneuver was imposed to measure the resistance of the entire respiratory system.

Preparation of single-cell suspensions from lungs and BALF and differential counting

Mouse lungs were diced into small pieces using razor blades and incubated for 1 h in digestion medium (RPMI-1640 with 1 mg/mL collagenase type 4, Sigma) at 37°C. The lung cells were then filtered and treated with red blood cell lysis buffer. BALF cells were acquired by administering 1 mL PBS supplemented with 2% FBS 3 times using a tracheal cannula. Lavage fractions were pooled together for total and differential cell counts. Differential cell counts were conducted with cytospin preparations after Giemsa staining and were validated by flow cytometric analysis using a BD Fortessa (BD Biosciences).

Transcriptome analysis

*i*NKT cells from *Acc1*$^{fl/fl}$ and *Cd4*-Cre*Acc1*$^{fl/fl}$ mice were sorted and total RNA was extracted using RNeasy with QIAshredders (Qiagen, Germantown, MD, USA). RNA quality and quantity were determined using an Agilent 2100 Bioanalyzer (Agilent Technologies, Santa Clara, CA, USA) and Nanodrop (Nanodrop Technologies, Wilmington, DE, USA). RNA-seq analyses were performed at the Theragen Bio Institute (Suwon, Korea). A Gene Set Enrichment Assay (GSEA) was performed to identify significant expression differences under the two biological conditions and to identify the gene classes that were overexpressed or underexpressed in *i*NKT cells from *Cd4*-Cre*Acc1*$^{fl/fl}$ mice relative to those from WT mice. The transcriptome data were from sorted *i*NKT cells from eight mice/group that were pooled together. We also analyzed transcriptome data from our previous study to compare the *i*NKT cells to conventional CD4^{+}T cells (GSE103190) [32]. These analyses were performed using GenePattern (https://genepattern.broadinstitute.org/).

Metabolome analysis

*i*NKT cells were sorted and pooled from eight WT mice, or eight *Cd4*-Cre*Accl1*$^{fl/fl}$ mice. The metabolites were extracted from each cell group as previously described [60, 61], followed by

MeOX and MTBSTFA derivatization. Metabolic profiling was performed by GC-MS/MS dynamic multiple reaction monitoring (dMRM) analyses using the Agilent 7890/7000 GC triple quadrupole mass spectrometer system. Gas chromatography was conducted using an Agilent J&W HP-5ms UI 15 m × 0.25 mm × 0.25 µm (P/N 19091S-431UI) capillary column. Helium was used as the carrier gas with a constant column flow rate of 1.5 mL min^{-1}. The initial oven temperature of 60°C was increased to 320°C at a rate of 10°C min^{-1}. The mass spectrometer was operated in the electron ionization mode at 70 eV. The analyses were performed in the dMRM mode. The area ratios of the analyte and the internal standard were used for the evaluation. The split/splitless injector temperature was set to 280°C. The samples were injected in the splitless mode with an autosampler Agilent 7683 A injector. Agilent MassHunter Data Acquisition Software (ver. B.04.00) and MassHunter Workstation Software for Quantitative Analysis (QQQ) were used for data acquisition and the quantitative analysis, respectively. The results were normalized to the *i*NKT-cell numbers and/or total protein concentrations.

Quantitative RT-PCR

To analyze gene-expression levels in the metabolic pathways, immune cells were sorted and pooled from four-eight mice/group, and used in the analysis. Total RNA was isolated with TRIzol reagent (Thermo Fisher Scientific) according to the manufacturer's protocol. RNA was reverse-transcribed into cDNA using Maloney murine leukemia virus reverse transcriptase Taq polymerase (Promega, Madison, WI, USA). For quantitative RT-PCR, gene-specific PCR products were quantified by an Applied Biosystems 7500 Sequence Detection System (Applied Biosystems, Foster City, CA, USA). The list of primers and their sequences used are summarized in Table S2. Gene-expression levels were normalized to those of *Actb* for mice and *ACTB* for humans.

Histology

Lung tissues were obtained from WT and J□18 KO mice that did or did not undergo transfer of *i*NKT cells from *Acc1*$^{fl/fl}$ and *Cd4*-Cre*Acc1*$^{fl/fl}$ mice during OVA- or HDM-induced asthma. The tissues were fixed in 10% formalin, embedded in paraffin, and sectioned, followed by staining with hematoxylin and eosin or periodic acid-Schiff (PAS). Lung inflammation and goblet cell hyperplasia were graded using a semi-quantitative scoring system as previously described [62, 63]. Briefly, inflammatory-cell numbers were graded as follows: 0: normal; 1: few cells; 2: a ring of inflammatory cells that was 1 cell-layer deep; 3: a ring of inflammatory cells that was 2–4 cell-layers deep; and 4: a ring of inflammatory cells that was >4 cell-layers deep. The goblet-cell numbers in the airway were graded as follows: 0: < 0.5% PAS-positive cells; 1: < 25%; 2: 25–50%; 3: 50–75%; and 4: > 75%. Two fields were counted for each slide and mean score was calculated for each group. Two pulmonary pathologists reviewed and analyzed representative images.

ECAR and OCR assays

*i*NKT cells were sorted from eight mice/group and pooled together. ECAR and OCR assays were performed using a Seahorse Extracellular Flux Analyzer XF24e (Seahorse Bioscience Inc., Santa Clara, CA, USA) according to the manufacturer's instructions. Briefly, the cells were seeded in a Seahorse plate and cultured overnight to 70–80% confluence. The culture medium was then replaced with cellular assay medium supplemented with 1 mM glutamine for the ECAR assay and 1 mM pyruvate, 2 mM glutamine, and 10 mM glucose for the OCR assay. The cells were incubated for 1 h in a CO_2-free incubator before measurement. The assays were performed according to the Seahorse protocols with final concentrations of 10 mM glucose, 2 μM oligomycin, and 50 mM 2-DG for ECAR, and 2 μM oligomycin, 1 μM carbonyl cyanide-4 (trifluoromethoxy) phenylhydrazone (FCCP), and 1 μM antimycin A for OCR. These assays were performed in at least three independent experiments on separate

days.

Pyrosequencing assay

Genomic DNA was converted with bisulfite by using the EZ DNA Methylation Kit (Zymo Research, Irvine, CA, USA) according to the manufacturer's protocol. PyroMarkTM software was used to design the pyrosequencing primers. In brief, bisulfite-converted DNA was subjected to PCR amplification in a total volume of 25 µL. DNA methylation was assessed using a PyroMark Q48 Autoprep system (Qiagen) and PyroMark Q48 Advanced CpG Reagents (Qiagen). The nucleotide dispensation order was generated by entering the sequences into the PyroMark Q48 Autoprep software ver. 2.4.2 (Qiagen). The methylation at each CpG site was determined using the PyroMark Q48 Autoprep software set in CpG mode. The mean methylation of all CpG sites within the target region was determined by using the methylation at the individual CpG sites.

Statistical analyses

GraphPad Prism 7 (GraphPad Software, La Jolla, CA, USA) was used for the statistical analyses and graphical display of the data. Unpaired 2-tailed t-tests or Mann-Whitney U test were performed to compare the groups. P values < 0.05 were considered statistically significant.

References

1. Allende, M.L. *et al.* S1P1 receptor expression regulates emergence of NKT cells in peripheral tissues. *FASEB J* **22**, 307-315 (2008).

2. Brossay, L. *et al.* CD1d-mediated recognition of an alpha-galactosylceramide by natural killer T cells is highly conserved through mammalian evolution. *J Exp Med* **188**, 1521-1528 (1998).

3. Abdollahi-Roodsaz, S. *et al.* Stimulation of TLR2 and TLR4 differentially skews the balance of T cells in a mouse model of arthritis. *The Journal of clinical investigation* **118**, 205-216 (2008).

4. Osuchowski, M.F. *et al.* Minimum Quality Threshold in Pre-Clinical Sepsis Studies (MQTiPSS): An International Expert Consensus Initiative for Improvement of Animal Modeling in Sepsis. *Shock* **50**, 377-380 (2018).

5. Ma, C. *et al.* Gut microbiome-mediated bile acid metabolism regulates liver cancer via NKT cells. *Science* **360** (2018).

6. Terabe, M. & Berzofsky, J.A. Tissue-Specific Roles of NKT Cells in Tumor Immunity. *Front Immunol* **9**, 1838 (2018).

7. Kim, H.Y. *et al.* NKT cells promote antibody-induced joint inflammation by suppressing transforming growth factor beta1 production. *J Exp Med* **201**, 41-47 (2005).

8. Akbari, O. *et al.* Essential role of NKT cells producing IL-4 and IL-13 in the development of allergen-induced airway hyperreactivity. *Nat Med* **9**, 582-588 (2003).

9. Manson, M.L. *et al.* IL-13 and IL-4, but not IL-5 nor IL-17A, induce

hyperresponsiveness in isolated human small airways. *J Allergy Clin Immun* **145**, 808-+ (2020).

10. Woo, Y.D., Koh, J., Kang, H.R., Kim, H.Y. & Chung, D.H. The invariant natural killer T cell-mediated chemokine X-C motif chemokine ligand 1-X-C motif chemokine receptor 1 axis promotes allergic airway hyperresponsiveness by recruiting CD103(+) dendritic cells. *J Allergy Clin Immunol* **142**, 1781-1792 e1712 (2018).

11. Akbari, O. *et al.* CD4+ invariant T-cell-receptor+ natural killer T cells in bronchial asthma. *N Engl J Med* **354**, 1117-1129 (2006).

12. Das, J. *et al.* Natural killer T cells and CD8+ T cells are dispensable for T cell-dependent allergic airway inflammation. *Nat Med* **12**, 1345-1346; author reply 1347 (2006).

13. Foell, D., Wittkowski, H., Vogl, T. & Roth, J. S100 proteins expressed in phagocytes: a novel group of damage-associated molecular pattern molecules. *Journal of leukocyte biology* **81**, 28-37 (2007).

14. Hamzaoui, A. *et al.* NKT cells in the induced sputum of severe asthmatics. *Mediators Inflamm* **2006**, 71214 (2006).

15. Pham-Thi, N. *et al.* Enhanced frequency of immunoregulatory invariant natural killer T cells in the airways of children with asthma. *J Allergy Clin Immunol* **117**, 217-218 (2006).

16. Thomas, S.Y., Lilly, C.M. & Luster, A.D. Invariant natural killer T cells in bronchial asthma. *N Engl J Med* **354**, 2613-2616; author reply 2613-2616 (2006).

17. Jung, J., Zeng, H. & Horng, T. Metabolism as a guiding force for immunity. *Nat Cell Biol* **21**, 85-93 (2019).

18. Ganeshan, K. & Chawla, A. Metabolic Regulation of Immune Responses. *Annual Review of Immunology, Vol 32* **32**, 609-634 (2014).

19. Yarosz, E.L., Chang, C.H. & Kumar, A. Metabolism in Invariant Natural Killer T Cells: An Overview. *Immunometabolism* **3** (2021).

20. Kim, Y.H., Kumar, A., Chang, C.H. & Pyaram, K. Reactive Oxygen Species Regulate the Inflammatory Function of NKT Cells through Promyelocytic Leukemia Zinc Finger. *J Immunol* **199**, 3478-3487 (2017).

21. Kumar, A. *et al*. Enhanced oxidative phosphorylation in NKT cells is essential for their survival and function. *P Natl Acad Sci USA* **116**, 7439-7448 (2019).

22. Al-Khami, A.A. *et al.* Fuelling the mechanisms of asthma: Increased fatty acid oxidation in inflammatory immune cells may represent a novel therapeutic target. *Clin Exp Allergy* **47**, 1170-1184 (2017).

23. Tibbitt, C.A. *et al*. Single-Cell RNA Sequencing of the T Helper Cell Response to House Dust Mites Defines a Distinct Gene Expression Signature in Airway Th2 Cells. *Immunity* **51**, 169-184 (2019).

24. Berod, L. *et al.* De novo fatty acid synthesis controls the fate between regulatory T and T helper 17 cells. *Nat Med* **20**, 1327-1333 (2014).

25. Soroosh, P. *et al*. Oxysterols are agonist ligands of RORgammat and drive Th17 cell differentiation. *Proc Natl Acad Sci U S A* **111**, 12163-12168 (2014).

26. Wang, C. *et al.* CD5L/AIM Regulates Lipid Biosynthesis and Restrains Th17 Cell Pathogenicity. *Cell* **163**, 1413-1427 (2015).

27. Wakil, S.J. & Abu-Elheiga, L.A. Fatty acid metabolism: target for metabolic syndrome. *Journal of lipid research* **50 Suppl**, S138-143 (2009).

28. Huang, S.C. *et al.* Cell-intrinsic lysosomal lipolysis is essential for alternative activation of macrophages. *Nat Immunol* **15**, 846-855 (2014).

29. Nakajima, T. *et al.* ACC1-expressing pathogenic T helper 2 cell populations facilitate lung and skin inflammation in mice. *J Exp Med* **218** (2021).

30. Endo, Y. *et al.* ACC1 determines memory potential of individual CD4(+) T cells by regulating de novo fatty acid biosynthesis. *Nat Metab* **1**, 261-275 (2019).

31. Lee, J. *et al.* Regulator of fatty acid metabolism, acetyl coenzyme a carboxylase 1, controls T cell immunity. *J Immunol* **192**, 3190-3199 (2014).

32. Oh, S.J., Ahn, J.Y. & Chung, D.H. Comparison of Invariant NKT Cells with Conventional T Cells by Using Gene Set Enrichment Analysis (GSEA). *Immune network* **11**, 406-411 (2011).

33. Hachem, P. *et al.* Alpha-galactosylceramide-induced iNKT cells suppress experimental allergic asthma in sensitized mice: role of IFN-gamma. *Eur J Immunol* **35**, 2793-2802 (2005).

34. Chandra, S. *et al.* A new mouse strain for the analysis of invariant NKT cell function. *Nat Immunol* **16**, 799-800 (2015).

35. Pajak, B. *et al.* 2-Deoxy-d-Glucose and Its Analogs: From Diagnostic to Therapeutic Agents. *Int J Mol Sci* **21** (2019).

36. Ahmadian, M. *et al.* PPARgamma signaling and metabolism: the good, the bad and the future. *Nat Med* **19**, 557-566 (2013).

37. Grygiel-Gorniak, B. Peroxisome proliferator-activated receptors and their ligands: nutritional and clinical implications--a review. *Nutr J* **13**, 17 (2014).

38. Moon, Y.A., Shah, N.A., Mohapatra, S., Warrington, J.A. & Horton, J.D. Identification of a mammalian long chain fatty acyl elongase regulated by sterol regulatory element-binding proteins. *J Biol Chem* **276**, 45358-45366 (2001).

39. Wolfrum, C., Borrmann, C.M., Borchers, T. & Spener, F. Fatty acids and hypolipidemic drugs regulate peroxisome proliferator-activated receptors alpha - and gamma-mediated gene expression via liver fatty acid binding protein: a signaling path to the nucleus. *Proc Natl Acad Sci U S A* **98**, 2323-2328 (2001).

40. Patil, R. *et al.* A ligand-induced structural change in fatty acid-binding protein 1 is associated with potentiation of peroxisome proliferator-activated receptor alpha agonists. *J Biol Chem* **294**, 3720-3734 (2019).

41. Hou, Y. *et al*. FABP5 controls macrophage alternative activation and allergic asthma by selectively programming long-chain unsaturated fatty acid metabolism. *Cell Rep* **41**, 111668 (2022).

42. Goto, Y. *et al*. Segmented filamentous bacteria antigens presented by intestinal dendritic cells drive mucosal Th17 cell differentiation. *Immunity* **40**, 594-607 (2014).

43. Lehmann, J.M. *et al.* An Antidiabetic Thiazolidinedione Is a High-Affinity Ligand for Peroxisome Proliferator-Activated Receptor Gamma(Ppar-Gamma). *Journal of Biological Chemistry* **270**, 12953-12956 (1995).

44. Masters, C.J., Reid, S. & Don, M. Glycolysis - New Concepts in an Old Pathway. *Molecular and cellular biochemistry* **76**, 3-14 (1987).

45. Roberts, L.D. *et al.* The contrasting roles of PPARdelta and PPARgamma in regulating the metabolic switch between oxidation and storage of fats in white adipose tissue. *Genome Biol* **12**, R75 (2011).

46. Panasyuk, G. *et al.* PPARgamma contributes to PKM2 and HK2 expression in fatty liver. *Nat Commun* **3**, 672 (2012).

47. Coman, C. *et al.* Simultaneous Metabolite, Protein, Lipid Extraction (SIMPLEX): A Combinatorial Multimolecular Omics Approach for Systems Biology. *Mol Cell Proteomics* **15**, 1453-1466 (2016).

48. Calvier, L. *et al.* PPARgamma Links BMP2 and TGFbeta1 Pathways in Vascular Smooth Muscle Cells, Regulating Cell Proliferation and Glucose Metabolism. *Cell Metab* **25**, 1118-1134 e1117 (2017).

49. Mao, A.P. *et al.* Multiple layers of transcriptional regulation by PLZF in NKT-cell development. *Proc Natl Acad Sci U S A* **113**, 7602-7607 (2016).

50. Fu, S. *et al.* Impaired lipid biosynthesis hinders anti-tumor efficacy of intratumoral iNKT cells. *Nature communications* **11**, 438 (2020).

51. Wohlfert, E.A., Nichols, F.C., Nevins, E. & Clark, R.B. Peroxisome proliferator-activated receptor gamma (PPAR gamma) and immunoregulation: Enhancement of regulatory T cells through PPAR gamma-dependent and -independent mechanisms. *Journal of Immunology* **178**, 4129-4135 (2007).

52. Klotz, L. *et al.* The nuclear receptor PPAR gamma selectively inhibits Th17 differentiation in a T cell-intrinsic fashion and suppresses CNS autoimmunity. *Journal of Experimental Medicine* **206**, 2079-2089 (2009).

53. Huang, Q. *et al.* Mechanistic Insights Into the Interaction Between Transcription Factors and Epigenetic Modifications and the Contribution to the Development of Obesity. *Front Endocrinol (Lausanne)* **9**, 370 (2018).

54. Furuhashi, M. & Hotamisligil, G.S. Fatty acid-binding proteins: role in metabolic diseases and potential as drug targets. *Nat Rev Drug Discov* **7**, 489-503 (2008).

55. Veerkamp, J.H. & van Moerkerk, H.T. Fatty acid-binding protein and its relation to fatty acid oxidation. *Molecular and cellular biochemistry* **123**, 101-106 (1993).

56. Barak, Y. & Lee, C.H. The Molecular Basis of PPAR Function. *PPAR Res* **2010**, 510530 (2010).

57. Tan, N.S. *et al.* Selective cooperation between fatty acid binding proteins and peroxisome proliferator-activated receptors in regulating transcription. *Mol Cell Biol* **22**, 5114-5127 (2002).

58. Shim, J.U. & Koh, Y.I. Increased Th2-like Invariant Natural Killer T cells in Peripheral Blood From Patients With Asthma. *Allergy Asthma Immun* **6**, 444-448 (2014).

59. Mayer, C.M. & Belsham, D.D. Palmitate attenuates insulin signaling and induces endoplasmic reticulum stress and apoptosis in hypothalamic neurons: rescue of resistance and apoptosis through adenosine 5' monophosphate-activated protein kinase activation. *Endocrinology* **151**, 576-585 (2010).

60. Faubert, B. *et al.* AMPK Is a Negative Regulator of the Warburg Effect and Suppresses Tumor Growth In Vivo. *Cell metabolism* **17**, 113-124 (2013).

61. Faubert, B. *et al.* Loss of the tumor suppressor LKB1 promotes metabolic reprogramming of cancer cells via HIF-1 alpha. *P Natl Acad Sci USA* **111**, 2554-2559 (2014).

62. Kujur, W., Gurram, R.K., Haleem, N., Maurya, S.K. & Agrewala, J.N. Caerulomycin A inhibits Th2 cell activity: a possible role in the management of asthma. *Sci Rep* **5**, 15396 (2015).

63. Myou, S. *et al.* Blockade of inflammation and airway hyperresponsiveness in

immune-sensitized mice by dominant-negative phosphoinositide 3-kinase-TAT. *J Exp Med* **198**, 1573-1582 (2003).

Acknowledgments

We would like to appreciate the NIH Tetramer Core Facility at the National Institute of Health, USA for providing PBS-57 loaded CD1d tetramers.

Declaration of interests

The authors declare no competing interests.

Author contributions

JK, YDW, and YHJ conducted the experiments; KCJ provided mice; CJP, KSH and CYS provided human samples and clinical information; KJH, KCJ, YKJ and HYK contributed to interpretation of results; DHC, JK, and YDW designed the experiments, interpreted data, and wrote the paper.

Funding Statement

This work was supported by the Basic Research Program through the National Research Foundation of Korea (NRF) funded by the MSIT (NRF-2020R1A4A1017515) and the National Research Foundation of Korea (NRF) grant funded by the Korea government (MSIT) (NRF-2020R1A2C2008312).

Figure legends

Figure 1. The fatty-acid synthesis pathway is upregulated in *i*NKT cells during murine allergic asthma.

(A–B) WT mice were subjected to OVA-induced asthma. (A) Schematic depiction of the OVA-induced allergic asthma model (left). The airway resistance of naïve, OVA-sensitized, and OVA-sensitized and OVA-challenged WT mice (right). (B) Gene expression of enzymes related to glycolysis, the TCA cycle, β-oxidation, and fatty-acid synthesis in lung *i*NKT cells that were sorted on d0, d7, and d17. The data shown in (A) and (B) are pooled data from four independent experiments (n = 8/group). (C) *In vitro* gene expression of enzymes related to glycolysis (*Hk2* and *Pkm2*), the TCA cycle (*Sdh2b* and *Idh1a*), and fatty-acid synthesis (*Acc1* and *Fasn*) in $CD8^+$ T, $CD4^+$ T, and *i*NKT cells before and after CD3/CD28 stimulation. Representative results from two independent experiments (n = 4/group) are shown. (D–I) *Cd4*-Cre*Accl1*$^{fl/fl}$ mice and the *Acc1*$^{fl/fl}$ control mice were subjected to OVA-induced asthma (D–F) or HDM-induced asthma (G–I). (D and G) Airway resistance. (E and H) Numbers and survival status of *i*NKT cells that were sorted from the lung by flow cytometry. (F and I) Cytokine expression in *i*NKT cells sorted from the lung. The data shown in (D–I) are pooled data from four independent experiments (n = 8/group). All data are presented as mean ± SEM. n.s, not significant. $*p < 0.05$, $**p < 0.01$, $***p < 0.001$, as determined by Unpaired 2-tailed t-tests.

Figure 2. ACC1 deficiency in murine *i*NKT cells associates with failure to develop α-GalCer-induced AHR.

Cd4-Cre*Acc1*$^{fl/fl}$ and *Acc1*$^{fl/fl}$ mice were administered α-GalCer intranasally. (A) Airway resistance. (B) Total immune cell numbers in the lungs and BALF. (C–D) Numbers of immune-cell subsets in the BALF (C) and lungs (D). (E–F) Expression levels of transcription factors (E) and cytokines (F) in the conventional $CD4^+$ T-cell population that was sorted from

the lungs. (G) Numbers and survival status of *i*NKT cells sorted from the lungs. (H) Cytokine expression in *i*NKT cells sorted from the lungs. All data are pooled from five independent experiments (n = 10/group) and presented as mean ± SEM. n.s, not significant. *$p < 0.05$, **$p < 0.01$, ***$p < 0.001$, as determined by Unpaired 2-tailed t-tests.

Figure 3. Adoptive transfer of WT, but not ACC1-deficient, *i*NKT cells restores the ability of NKT-knockout mice to develop OVA-induced asthma.

*i*NKT cells sorted from naïve *Cd4*-Cre*Acc1*$^{fl/fl}$ and *Acc1*$^{fl/fl}$ mice were adoptively transferred into naïve WT and Jα18 KO mice, after which OVA-induced asthma was initiated. (A) Airway resistance. (B) Total inflammatory cell numbers in the lungs and BALF. (C–D) Numbers of immune-cell subsets in BALF (C) and lungs (D). (E–F) Expression levels of transcription factors (E) and cytokines (F) in CD4^{+} T cells sorted from the lungs. (G) Cytokine expression in *i*NKT cells sorted from the lungs. (H–I) Numbers (H) and survival status (I) of *i*NKT cells from the lungs. (J) Representative histological lung section images and histological scores. The data in (A–J) are pooled data from four independent experiments (n = 8/group). All data are presented as mean ± SEM. n.s, not significant. *$p < 0.05$, **$p < 0.01$, ***$p < 0.001$, as determined by Unpaired 2-tailed t-tests.

Figure 4. The high glycolytic capacity of ACC1-deficient *i*NKT cells associates with their enhanced cell death.

*i*NKT cells were sorted from the liver of naïve *Cd4*-Cre*Acc1*$^{fl/fl}$ and *Acc1*$^{fl/fl}$ mice and used directly in the experiments. The two *i*NKT-cell preparations were compared. (A) Volcano plot of the gene expression. (B) Signature gene expression, as determined by Gene Set Enrichment Analysis (GSEA). (C) Heat map of the fatty-acid synthesis, glycolysis, cell death, and cytokine genes. (D) Metabolome data map of the glycolysis, TCA cycle, and fatty-acid synthesis metabolites. (E) Seahorse extracellular flux analysis of ECAR and OCR. (F)

Expression of glycolysis-related (*Hk2*, *Pkm2*) and gluconeogenesis-related (*Fbp1*, *G6pase*) genes. (G) 2-NBDG uptake. (H) GLUT1 expression. (I) Correlation between *i*NKT-cell death and maximal glycolytic activity. (J–K) The *i*NKT cells were treated with 2-DG to inhibit glycolysis. The effect of 2-DG on cell death (J) and intrinsic cell death-related gene expression (K) was then determined. In (A–D), the *i*NKT cells were from 8 mice/group. The data in (D) are presented as mean ± SEM. The data in (E–K) are pooled data from five independent experiments (n = 5/group) and are presented as mean ± SEM. n.s, not significant. $*p < 0.05$, $**p < 0.01$, $***p < 0.001$, as determined by Unpaired 2-tailed t-tests.

Figure 5. Low PPARγ expression in ACC1-deficient *i*NKT cells contributes to their enhanced cell death

*i*NKT cells sorted from the liver of naïve *Cd4*-Cre*Acc1*$^{fl/fl}$ and *Acc1*$^{fl/fl}$ mice were either used directly in the experiment (A) or cultured with and/or without anti-CD3/CD28 with and without the indicated additives (C–H). (A) Heatmap of the transcription factor genes in the uncultured *i*NKT-cell preparations. (B) CD3/CD28-stimulated and unstimulated *i*NKT cells were cultured with and without pioglitazone and *Pparg*, *Cepba*, *Fbp1*, *G6pase*, *Hk2*, and *Pkm2* expression was examined. (C–D) Unstimulated *i*NKT cells were cultured with and without pioglitazone and 2-NBDG uptake, GLUT1 expression (C), and cell death (D) were examined. (E) CD3/CD28-stimulated and unstimulated *i*NKT cells were cultured with and without palmitate and/or FABP inhibitor and *Pparg*, *Cepba*, *Fbp1*, *G6pase*, *Hk2*, and *Pkm2* expression was examined. (F) Unstimulated *i*NKT cells were cultured with and without palmitate and *Fabp1*, *Fabp3*, and *Fabp5* expression was examined. (G–H) Unstimulated *i*NKT cells were cultured with and without palmitate and/or FABP inhibitor and PPARγ expression (G), 2-NBDG uptake, and cell death (H) were examined. (I) Graphical abstract of ACC1-FABP-PPARγ in *i*NKT cells are shown. The data in (B–H) are pooled data from four independent experiments (n = 4/group) and are presented as mean ± SEM. n.s, not significant.

*$p < 0.05$, **$p < 0.01$, ***$p < 0.001$, as determined by Unpaired 2-tailed t-tests.

Figure 6. Pretreatment of ACC1-deficient *i*NKT cells with PPARγ agonist or exogenous fatty acid restores OVA-induced asthma.

*i*NKT cells sorted from naïve *Cd4*-Cre*Acc1*$^{fl/fl}$ and *Acc1*$^{fl/fl}$ mice were pretreated with and without pioglitazone or palmitate and then adoptively transferred into naïve WT and Jα18 KO mice. OVA-induced asthma was then initiated. (A) Airway resistance. (B) Representative histological images and histological scores of lung sections. (C) Total immune cell numbers in the lungs and BALFs. (D–E) Immune-cell subsets in the BALFs (D) and lungs (E). (F–G) Transcription factor (F) and cytokine (G) expression in the total CD4$^+$ T-cell population from the lungs. (H) Cell numbers and survival status of the lung *i*NKT cells. (I) Cytokine expression in the lung *i*NKT cells. (J) PPARγ, 2-NBDG, and GLUT1 expression in the lung *i*NKT cells. The data are pooled from four independent experiments (n = 8/group) and are presented as mean ± SEM. n.s, not significant. *$p < 0.05$, **$p < 0.01$, ***$p < 0.001$, as determined by Unpaired 2-tailed t-tests.

Legends for supplementary figures

Figure S1. *Cd4*-Cre*Acc1*$^{fl/fl–}$ mice fail to develop airway resistance in the HDM-induced asthma model

(A) Gene set enrichment analysis (GSEA) in *i*NKT versus CD4$^+$ T cells. *Acc1*$^{fl/fl}$ and *Cd4*-Cre*Accl1*$^{fl/fl}$ mice were intranasally challenged with OVA (B-F) or HDM (G-K), and various parameters were measured. (B and G). Total cell counts from the lungs and BALs (C, D, H, I). Estimation of immune cell subsets in the BALs (C and H) and lungs (D and I) via flow cytometry (E, F, J, K). Expression levels of transcription factors (E and J) and cytokines (F and K) in CD4$^+$ T (excluding *i*NKTs) cells sorted from lungs. Data were pooled from four independent experiments with n = 8 per group and presented as means ± SEMs. n.s, not

significant. *$p < 0.05$, **$p < 0.01$, ***$p < 0.001$ as determined by Unpaired 2-tailed t-tests

Figure S2. Deficiency of ACC1 in *i*NKT cells perturbed their thymic development and peripheral homeostasis in cell intrinsic manner

(A) The percentages of *i*NKT cells in the thymi, spleens, and livers from *Cd4*-Cre*Acc1*$^{fl/fl}$ and *Acc1*$^{fl/fl}$ mice were measured via flow cytometry. (B) Analysis of CD4$^+$ SP thymocytes, CD8$^+$ SP thymocytes, CD4$^+$CD8$^+$ DP thymocytes, CD4$^-$CD8$^-$ DN thymocytes, and CD8$^+$ T, CD4$^+$ T cells from the spleens of *Cd4*-Cre*Acc1*$^{fl/fl}$ and *Acc1*$^{fl/fl}$ mice. (C) Percentages of NKT1s, NKT2s, and NKT17s and developmental stages of *i*NKT cells from the thymus of *Cd4*-Cre*Acc1*$^{fl/fl}$ and *Acc1*$^{fl/fl}$ mice were measured via flow cytometry. (A-C) Data were pooled from four independent experiments with n = 4 per group. (D) Mixed bone marrow chimeras were generated by adoptive transfer of a mixture of WT CD45.1 bone marrow and CD45.2 *Cd4*-Cre*Acc1*$^{fl/fl}$ bone marrow into irradiated WT mice. To investigate the reconstitution, CD1d tetramer$^+$ *i*NKT cells were stained with CD45.1 and CD45.2 antibodies via flow cytometry. (E-F) The percentages of *i*NKT cells in the thymi, spleens, and livers (E) and of CD4$^+$SP, CD8$^+$SP, CD4$^+$CD8$^+$DP, and CD4$^-$CD8$^-$DN thymocytes and splenic CD4$^+$ T, CD8$^+$ T cells, CD3e$^+$ T cells, B cells (F) were measured via flow cytometry. (G-H) *i*NKT cells sorted from the livers of *Cd4*-Cre*Acc1*$^{fl/fl}$ and *Acc1*$^{fl/fl}$ mice were stimulated with CD3/CD28 antibodies. (G) The levels of IL-4 and IFN-γ in the culture supernatants were assessed by ELISA. (H) Expression of CD69 was estimated via flow cytometry. (D-H) Data were pooled from three independent experiment with n = 30 per group and presented as means ± SEMs. n.s, not significant. *$p < 0.05$, **$p < 0.01$, ***$p < 0.001$ as determined by Unpaired 2-tailed t-tests

Figure S3. ACC1 deficiency does not affect epigenetic modification of *Pparg* in *i*NKT cells

(A) Schematic structure of the *Pparg* promoter and identification of the CpG-enriched regions. *Pparg* methylation was measured via pyrosequencing. (B and C) Expression levels of *Pparg*, *Hk2*, *Bcl2*, *Bak* (B), and cell death (C) of *i*NKT cells from *Cd4*-Cre*Acc1*$^{fl/fl}$ or *Acc1*$^{fl/fl}$ mice in the presence or absence of HDAC inhibitor treatment. Data were pooled from four independent experiments with n = 4 per group and presented as means ± SEMs. n.s, not significant. *$p < 0.05$, **$p < 0.01$, ***$p < 0.001$ as determined by Unpaired 2-tailed t-tests

Figure S4. Adoptive transfer of Acc1-deficient *i*NKT cells pretreated with exogenous fatty acid or PPAR-γ agonist into *i*NKT cell-deficient mice (Jα18 KO) restores AHR in the HDM-induced asthma model

(A) Airway resistance was measured in WT, Jα18KO, and Jα18KO mice adoptively transferred with *i*NKT cells from *Acc1*$^{fl/fl}$ or *Cd4*-Cre*Acc1*$^{fl/fl}$ mice in the presence or absence of pioglitazone or palmitate treatment upon HDM challenge. (B) Representative histological images of lung sections from the indicated mouse groups challenged with HDM. (C-E) Total cell numbers in the lungs and BALs were counted (C), and subsets of immune cells in the BALs (D) and lungs (E) were estimated via flow cytometry. (F-G) Expression levels of transcription factors (F) and cytokines (G) were measured in CD4$^+$ T cells sorted from the lungs of mice with OVA-induced asthma. (H) Expression levels of cytokines were measured in *i*NKT cells sorted from the lungs of each mouse group. Data were pooled from four independent experiments with n = 8 per group and presented as means ± SEMs. n.s, not significant. *$p < 0.05$, **$p < 0.01$, ***$p < 0.001$ as determined by Unpaired 2-tailed t-tests

Figure S5. Genes for fatty acid metabolism are highly expressed in *i*NKT cells from PBMCs of patients with allergic asthma

(A and B) The expression levels of *ACC1*, *FASN*, *PPARG* (A), *HK2*, and *FBP1* (B) in CD8$^+$ T, CD4$^+$ T, regulatory T cells, and *i*NKT cells from peripheral blood samples of healthy

donors and patients with non-allergic asthma or allergic asthma (n = 10 per group). Data are presented as means ± SEMs. n.s, not significant. *$p < 0.05$, **$p < 0.01$, ***$p < 0.001$ as determined by Mann-Whitney U test

Table S1. List of reagents used for flow cytometry

Antibody/Reagent	Catalogue #	Clone	Company
PerCP/Cyanine5.5 anti-mouse CD45	103132	30-F11	BioLegend
PE/Cy7 anti-mouse CD11c	117318	N418	BioLegend
APC anti-mouse F4/80	123116	BM8	BioLegend
PE anti-mouse/human CD11b	101208	M1/70	BioLegend
FITC anti-mouse F4/80	123108	BM8	BioLegend
PE anti-mouse CD170 (Siglec-F)	155506	S17007L	BioLegend
Zombie Aqua™ Fixable Viability Kit	423101		BioLegend
Brilliant Violet 421™ anti-mouse/human CD11b	101236	M1/70	BioLegend
PE – Annexin V	640947	-	BioLegend
PE- anti-mouse PLZF	145803	Mag.21F7	BioLegend
PBS 57 – APC conjugated anti-mouse CD1d tetramer	-	-	NIH Tetramer Facility
PerCP anti-mouse CD45.1	110726	A20	BioLegend
Alexa Fluor® 700 anti-mouse CD45.2	109822	104	BioLegend
PE/Cy7 anti-mouse TCR β chain	109222	H57-597	BioLegend
APC anti-mouse CD86	105012	GL-1	BioLegend
FITC anti-mouse CD80	104706	16-10A1	BioLegend
PE/Cy7 anti-mouse CD69	104511	H1.2F3	BioLegend
FITC anti-mouse GLUT1	Sc-377228	A-4	Santa Cruz
FITC anti-mouse Ly-6G	127606	1A8	BioLegend
PE anti-mouse CD19	152408	1D3/CD19	BioLegend
APC anti-mouse CD4	100516	RM4-5	BioLegend
FITC anti-mouse CD8a	100706	53-6.7	BioLegend
PE anti-mouse FOXP3	126404	MF-14	BioLegend
Ovalbumin, Fluorescein Conjugate	O23020		ThermoFisher Scientific
PerCP anti-mouse NK-1.1	108725	PK136	BioLegend
APC anti-mouse/human CD44	103011	IM7	BioLegend
FITC anti-mouse BrdU	347583	B44	BD
PE anti-mouse CD24	553261	M1/69	BD Bioscience
Brilliant Violet 421™ anti-mouse CD62L	104435	MEL-14	BioLegend
PE anti-mouse CD64 (FCγRI)	139303	X54-5/7.1	BioLegend
Brilliant Violet 421™ anti-mouse Ly-6C	128031	HK1.4	BioLegend
PE/Cy7 Armenian Hamster IgG Isotype Ctrl	400921	HTK888	BioLegend
FITC Rat IgG2a, κ Isotype Ctrl	400505	RTK2758	BioLegend
PE Rat IgG2a, κ Isotype Ctrl	400507	RTK2758	BioLegend
Brilliant Violet 421™ Rat IgG2b, κ Isotype Ctrl	400639	RTK4530	BioLegend
PerCP/Cyanine5.5 anti-mouse IL-4	504123	11B11	BioLegend
PE anti-mouse IL-13	159403	W17010B	BioLegend
APC anti-human CD25	302609	BC96	BioLegend
FITC anti-human CD4	317407	OKT4	BioLegend

Table S2. Primer sequences used for real-time PCR

Species	Gene	F/R	Sequence
Mouse	Acox1	F	CTG CCA AGG GAC TCC AGA GCA GCT
Mouse	Acox1	R	GAC ATG GAC ACA TCC ACC ATG CAG
Mouse	Fasn	F	AGC GGC CAT TTC CAT TGC CC
Mouse	Fasn	R	CCA TGC CCA GAG GGT GGT TG
Mouse	Acc1	F	ACA GTG GAG CTA GAA TTG GAC
Mouse	Acc1	R	ACT TCC CGA CCA AGG ACT TTG
Mouse	PPAR-gamma	F	GTG ATG GAA GAC CAC TCG CAT T
Mouse	PPAR-gamma	R	CCA TGA GGG AGT TAG AAG GTT C
Mouse	Tbx21	F	TTCCCATTCCTGTCCTTCAC
Mouse	Tbx21	R	CCACATCCACAAACATCCTG
Mouse	Gata3	F	GGAAACTCCGTCAGGGCTA
Mouse	Gata3	R	AGAGATCCGTGCAGCAGAG
Mouse	Rorc	F	TGA GGC CAT TCA GTA TGT GG
Mouse	Rorc	R	CTT CCA TTG CTC CTG CTT TC
Mouse	Foxp3	F	CCC AGG AAA GAC AGC AAC CTT
Mouse	Foxp3	R	TTC TCA CAA CCA GGC CAC TTG
Mouse	Hk2	F	AGA GAA CAA GGG CGA GGA G
Mouse	Hk2	R	GGA AGC GGA CAT CAC AAT C
Mouse	g6pase	F	CCA TGC AAA GGA CTA GGA ACA A
Mouse	g6pase	R	TAC CAG GGC CGA TGT CAA C
Mouse	Fbp1	F	CCA TCA TAA TCG AAC CTG AG
Mouse	Fbp1	R	CTT CTC AGA AGG CTC ATC AG
Mouse	Sdhb	F	CTA AAT AAG TGC GGA CCT ATG G
Mouse	Sdhb	R	AGT ATT GCC TCC GTT GAT GTT C
Mouse	Cpt1a	F	CCA TCC TGT CCT GAC AAG GTT TAG
Mouse	Cpt1a	R	CCT CAC TTC TGT TAC AGC TAG CAC
Mouse	Pkm2	F	CTG GCT CAG AAG ATG ATG ATC G
Mouse	Pkm2	R	CTT GGT GAG CAC GAT AAT GG

Mouse	cEBPa	F	CAA AGC CAA GAA GTC GGT GGA
Mouse	cEBPa	R	TCA TTG TGA CTG GTC AAC TCC AGC
Mouse	Bak1	F	ATA TTA ACC GGC GCT ACG AC
Mouse	Bak1	R	AGG CGA TCT TGG TGA AGA GT
Mouse	Bax	F	TAG CAA ACT GGT GCT CAA
Mouse	Bax	R	TCT TGG ATC CAG ACA AGC AG
Mouse	Bcl-2	F	CTC GTC GCT ACC GTC GTG ACT TCG
Mouse	Bcl-2	R	CAG ATG CCG GTT CAG GTA CTC AGT C
Mouse	Bcl-XL	F	TGG AGT AAA CTG GGG GTC GCA TCG
Mouse	Bcl-XL	R	AGC CAC CGT CAT GCC CGT CAG G
Mouse	GAPDH	F	GGGAAGCTCACTGGCATGG
Mouse	GAPDH	R	CTTCTTGATGTCATCATACTTGGCAG
Mouse	IFN-r	F	CGG CAC AGT CAT TGA AAG CCT A
Mouse	IFN-r	R	GTT GCT GAT GGC CTG ATT GTC
Mouse	IL-4	F	TCA ACC CCC AGC TAG TTG TC
Mouse	IL-4	R	TGT TCT TCG TTG CTG TGA GG
Mouse	IL-5	F	CTC TGT TGA CAA GCA ATG AGA CG
Mouse	IL-5	R	TCT TCA GTA TGT CTA GCC CCT G
Mouse	IL-13	F	CCT GGC TCT TGC TTG CCT T
Mouse	IL-13	R	GGT CTT GTG TGA TGT TGC TCA
Mouse	IL-17a	F	GGT CTT GTG TGA TGT TGC TCA
Mouse	IL-17a	R	GGG TCT TCA TTG CGG TGG AGA G
Mouse	mFAPB1 F	F	AGG AGT GCG AAC TGG AGA CCA T
Mouse	mFAPB1 R	R	GTC TCC ATT GAG TTC AGT CAC GG
Mouse	mFAPB3 F	F	AGA GTT CGA CGA GGT GAC AGC A
Mouse	mFAPB3 R	R	TTG TCT CCT GCC CGT TCC ACT T
Mouse	mFAPB5 F	F	GAC GAC TGT GTT CTC TTG TAA CC
Mouse	mFAPB5 R	R	TGT TAT CGT GCT CTC CTT CCC G
Human	PPARg	F	AGT CCT CAC AGC TGT TTG CCA AGC
Human	PPARg	R	GAG CGG GTG AAG ACT CAT GTC TGT

			C
Human	h PPARG F	F	AGC CTG CGA AAG CCT TTT GGT G
Human	h PPARG R	R	GGC TTC ACA TTC AGC AAA CCT GG
Human	hBActin F	F	TCC CTG GAG AAG AGC TAC GA
Human	hBActin R	R	AGC ACT GTG TTG GCG TAC AG
Human	h-ACC1 F	F	ATG GGC GGA ATG GTC TCT TTC
Human	h-ACC1 R	R	TGG GGA CCT TGT CTT CAT CAT
Human	h-FASN F	F	GGA GGT GGT GAT AGC CGG TAT
Human	h-FASN R	R	GGG TAA TCC ATA GAG CCC AG
Human	h HK2 F	F	GAG TTT GAC CTG GAT GTG GTT GC
Human	h HK2 R	R	CCT CCA TGT AGC AGG CAT TGC T
Human	GAPDH	F	CAT GTT CGT CAT GGG GTG AAC CA
Human	GAPDH	R	AGT GAT GGC ATG GAC TGT GGT CAT

Figure 1

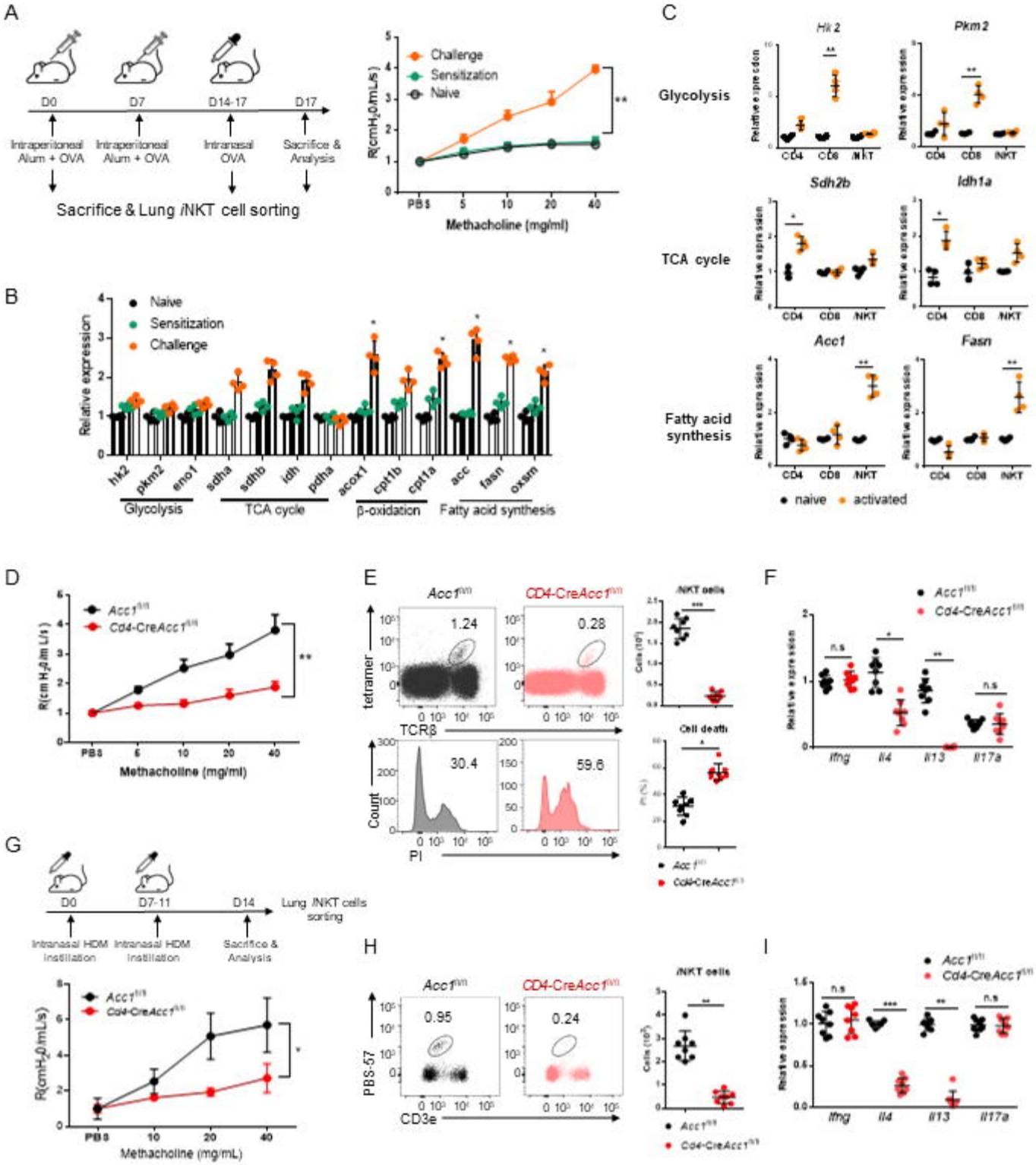
A
D0
D7
D14-17
D17
Intraperitoneal Alum + OVA
Intraperitoneal Alum + OVA
Intranasal OVA
Sacrifice & Analysis
Sacrifice & Lung iNKT cell sorting
Challenge
Sensitization
Naive
Methacholine (mg/ml)
B
Naive
Sensitization
Challenge
Relative expression
hk2
pkm2
eno1
sdha
sdhb
idh
pdha
acox1
cpt1b
cpt1a
acc
fasn
oxsm
Glycolysis
TCA cycle
β-oxidation
Fatty acid synthesis
C
Glycolysis
TCA cycle
Fatty acid synthesis
Hk2
Pkm2
Sdh2b
Idh1a
Acc1
Fasn
CD4
CD8
iNKT
naive
activated
D
Acc1
Methacholine (mg/ml)
E
Acc1
CD4-CreAcc1
tetramer
TCRβ
Count
PI
iNKT cells
Cell death
F
Acc1
Cd4-CreAcc1
Ifng
Il4
Il13
Il17a
G
D0
D7-11
D14
Lung iNKT cells sorting
Intranasal HDM instillation
Intranasal HDM instillation
Sacrifice & Analysis
Methacholine (mg/mL)
H
Acc1
CD4-CreAcc1
PBS-57
CD3e
iNKT cells
I
Acc1
Cd4-CreAcc1
Ifng
Il4
Il13
Il17a

Figure 2

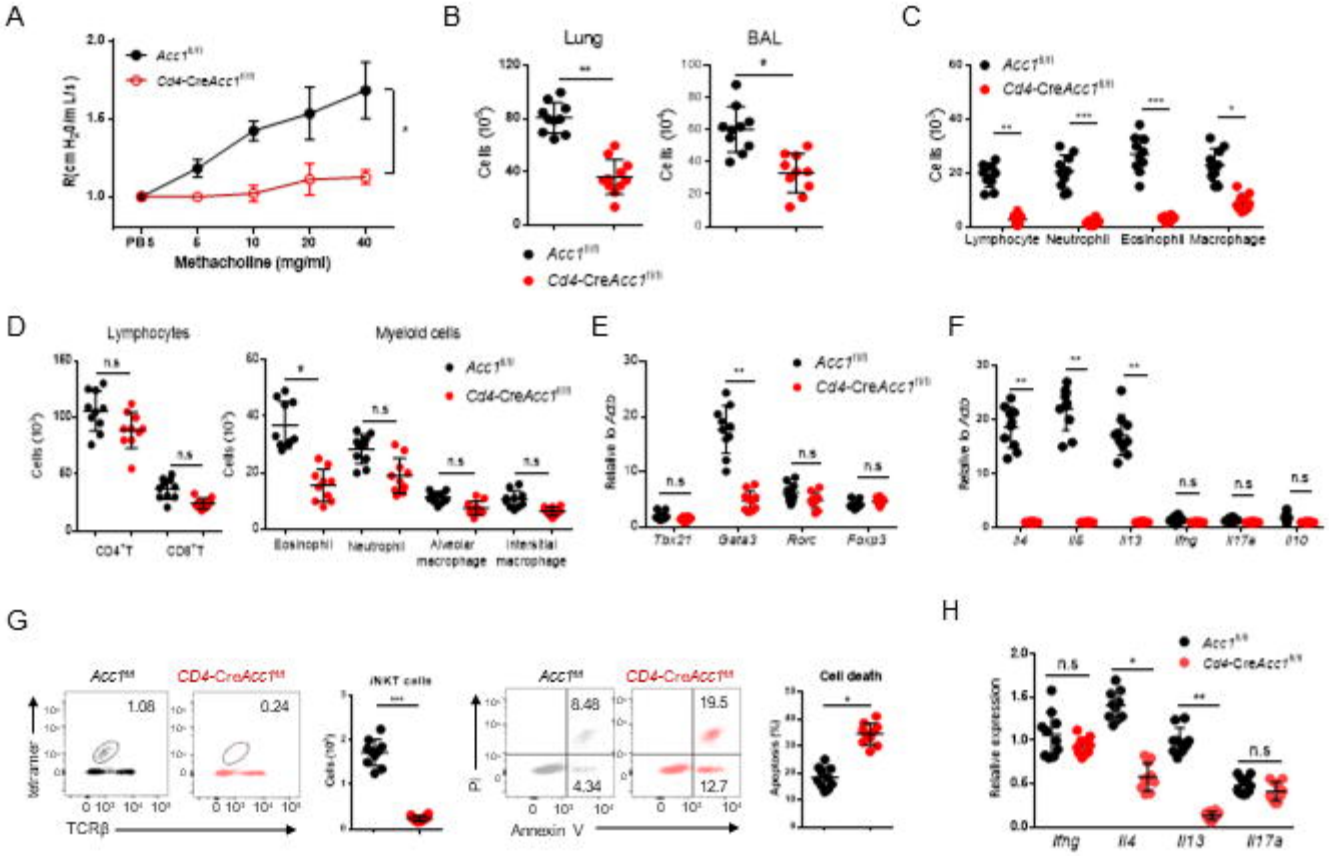
A
Acc1fl/fl
Cd4-CreAcc1fl/fl
R(cm H2O/ml/s)
PBS
5
10
20
40
Methacholine (mg/ml)
B
Lung
BAL
Cells (10⁴)
Acc1fl/fl
Cd4-CreAcc1fl/fl
C
Cells (10⁴)
Lymphocyte
Neutrophil
Eosinophil
Macrophage
D
Lymphocytes
Myeloid cells
Cells (10⁴)
n.s
CD4⁺T
CD8⁺T
Eosinophil
Neutrophil
Alveolar macrophage
Interstitial macrophage
E
Relative to Actb
Tbx21
Gata3
Rorc
Foxp3
F
Relative to Actb
Il4
Il5
Il13
Ifng
Il17a
Il10
G
Acc1fl/fl
CD4-CreAcc1fl/fl
1.08
0.24
Mitramycin
TCRβ
iNKT cells
Cells (10⁴)
8.48
4.34
19.5
12.7
PI
Annexin V
Cell death
Apoptosis (%)
H
Relative expression
n.s
Ifng
Il4
Il13
Il17a

Figure 3

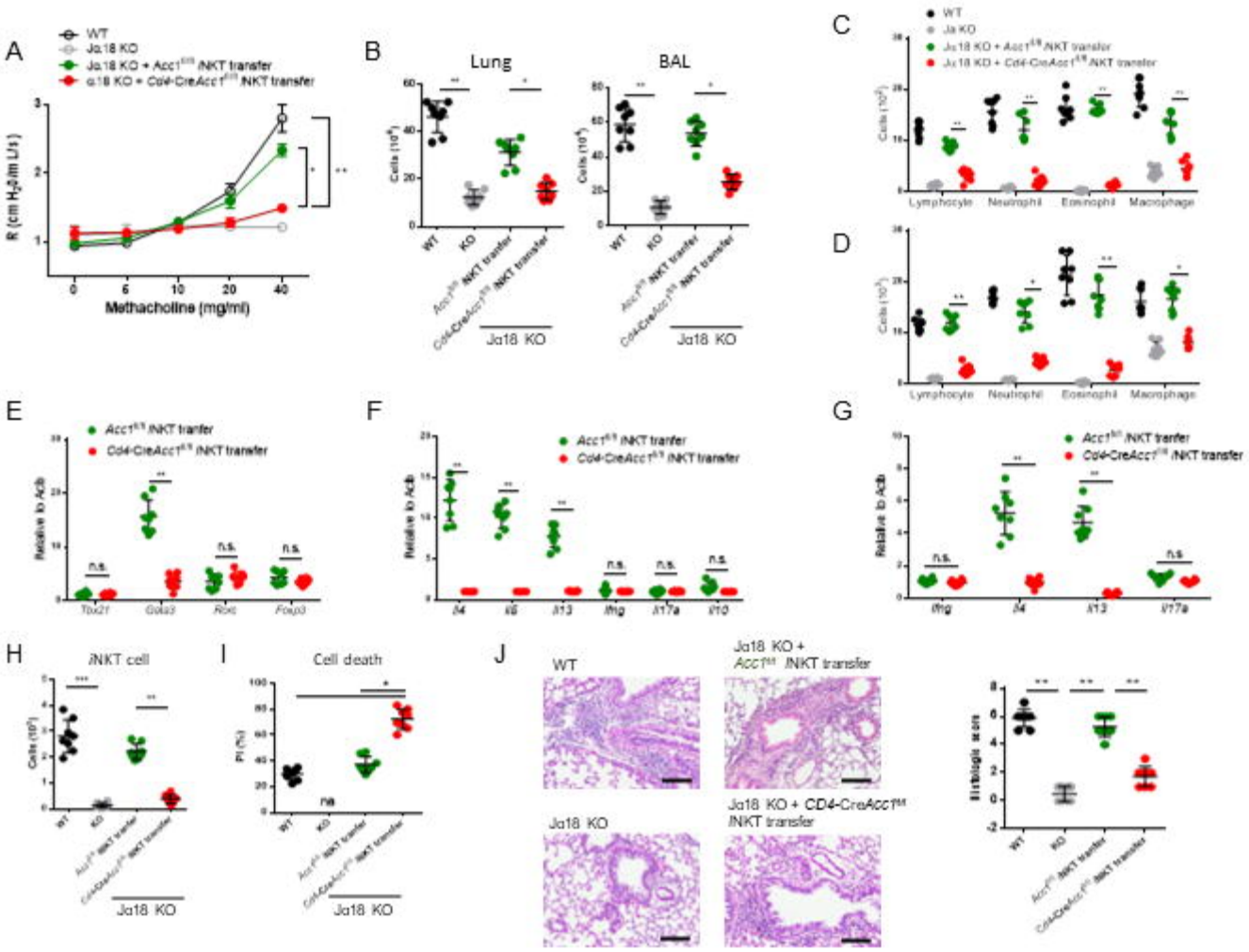
A
WT
Ja18 KO
Ja18 KO + Acc1 iNKT transfer
Ja18 KO + Cd4-CreAcc1 iNKT transfer
R (cm H2O/m L/s)
Methacholine (mg/ml)
B
Lung
BAL
Cells (10⁴)
WT
KO
Acc1 iNKT transfer
Cd4-CreAcc1 iNKT transfer
Ja18 KO
C
D
Lymphocyte
Neutrophil
Eosinophil
Macrophage
E
F
G
Relative to Actb
Tbx21
Gata3
Rorc
Foxp3
Il4
Il5
Il13
Ifng
Il17a
Il10
n.s.
H
iNKT cell
Cells (10⁴)
I
Cell death
PI (%)
na
J
WT
Ja18 KO + Acc1 iNKT transfer
Ja18 KO
Ja18 KO + CD4-CreAcc1 iNKT transfer
Histologic score

Figure 4

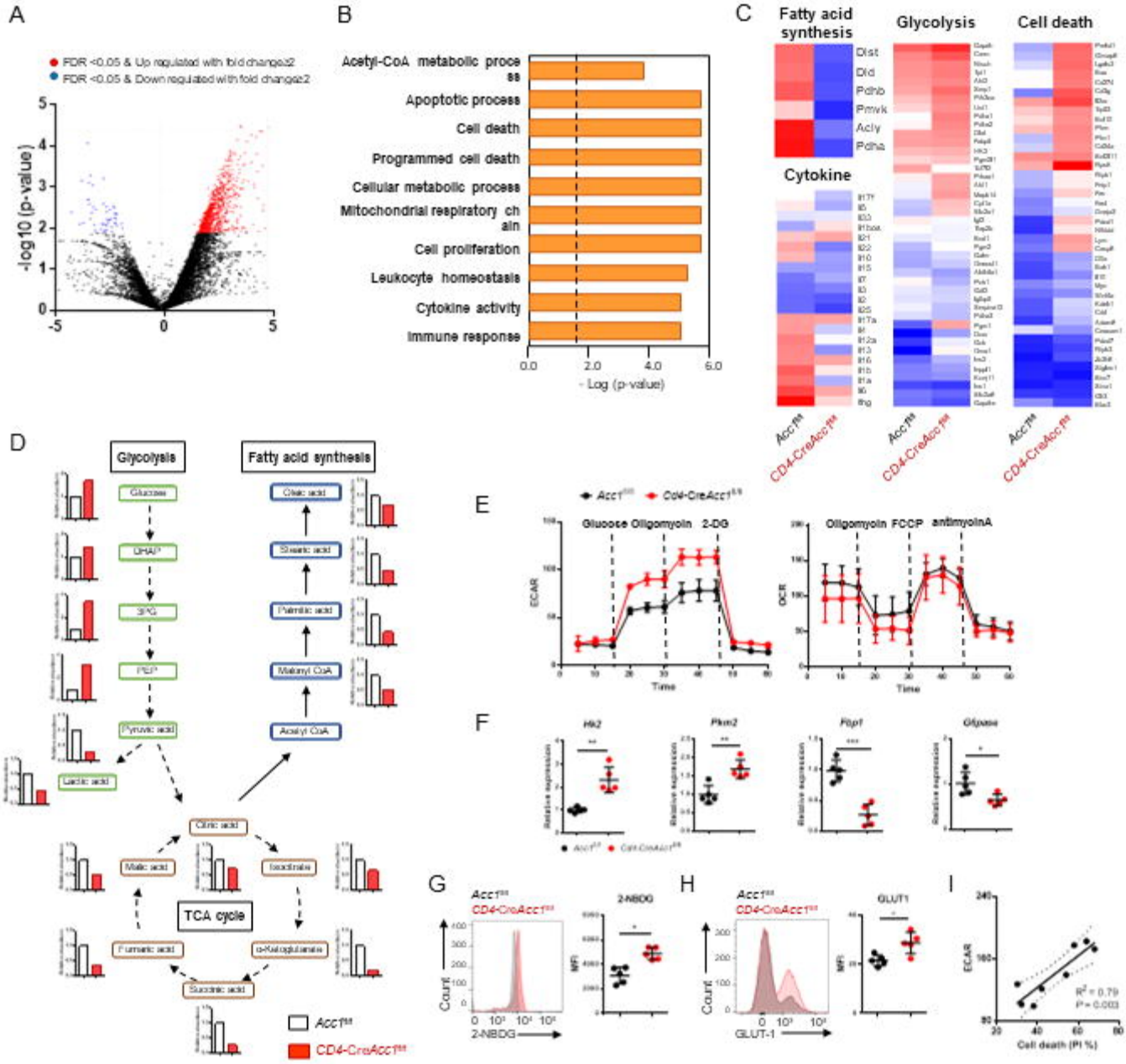
A
FDR <0.05 & Up regulated with fold change≥2
FDR <0.05 & Down regulated with fold change≥2
-log10 (p-value)
B
Acetyl-CoA metabolic process
Apoptotic process
Cell death
Programmed cell death
Cellular metabolic process
Mitochondrial respiratory chain
Cell proliferation
Leukocyte homeostasis
Cytokine activity
Immune response
- Log (p-value)
C
Fatty acid synthesis
Glycolysis
Cell death
Cytokine
Dlst
Dld
Pdhb
Pmvk
Acly
Pdha
Acc1fl/fl
CD4-CreAcc1fl/fl
D
Glycolysis
Fatty acid synthesis
Glucose
G6P
Pyruvic acid
Lactic acid
Oleic acid
Stearic acid
Palmitic acid
Malonyl CoA
Acetyl CoA
Citric acid
Malic acid
Isocitrate
TCA cycle
Fumaric acid
α-Ketoglutarate
Succinic acid
Acc1fl/fl
CD4-CreAcc1fl/fl
E
Acc1fl/fl
Cd4-CreAcc1fl/fl
Glucose Oligomycin 2-DG
Oligomycin FCCP antimycinA
ECAR
OCR
Time
F
Hk2
Pkm2
Fbp1
G6pase
Relative expression
G
Acc1fl/fl
CD4-CreAcc1fl/fl
2-NBDG
Count
MFI
H
GLUT1
GLUT-1
I
ECAR
Cell death (PI %)
R² = 0.79
P = 0.003
J
+PBS
+2-DG
6.58
5.22
6.85
6.05
17.6
12.3
8.04
11.8
Annexin V
Apoptosis (%)
+ 2-DG
K
Intrinsic death related genes
Relative expression
Bax
Bak1
Bcl2
Bcl-xl
Pro-apoptotic
Anti-apoptotic

Figure 5

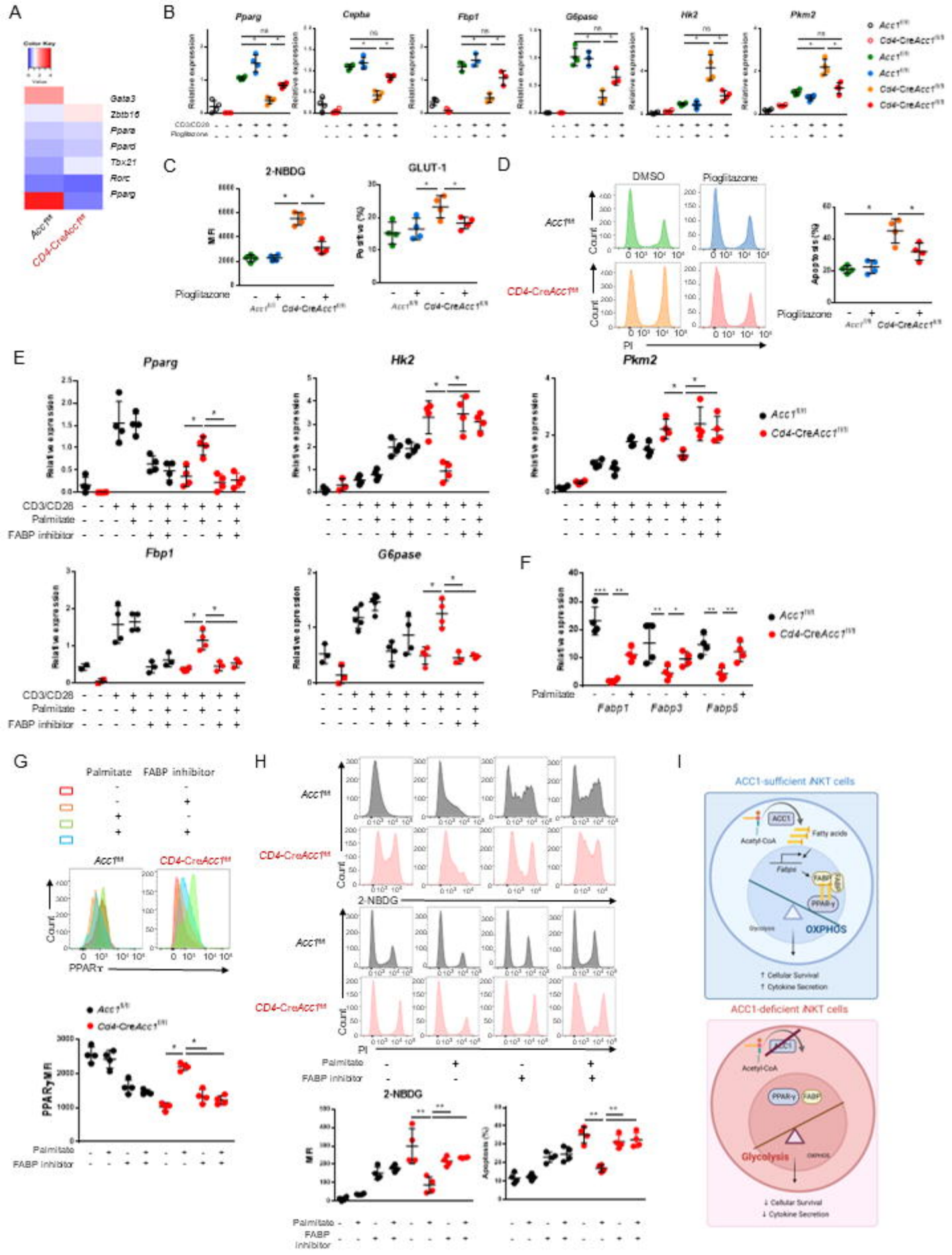
A
Color Key
Value
Gata3
Zbtb16
Pparα
Pparδ
Tbx21
Rorc
Pparγ
Acc1fl/fl
CD4-CreAcc1fl/fl
B
Pparg
Cebpa
Fbp1
G6pase
Hk2
Pkm2
Relative expression
ns
CD3/CD28
Pioglitazone
Acc1fl/fl
CD4-CreAcc1fl/fl
C
2-NBDG
GLUT-1
MFI
Positive (%)
Pioglitazone
D
DMSO
Pioglitazone
Count
PI
Apoptosis (%)
E
Palmitate
FABP inhibitor
F
Fabp1
Fabp3
Fabp5
G
PPARγ
PPARγMFI
H
2-NBDG
I
ACC1-sufficient iNKT cells
ACC1
Acetyl-CoA
Fatty acids
Fabps
FABP
PPAR-γ
Glycolysis
OXPHOS
↑ Cellular Survival
↑ Cytokine Secretion
ACC1-deficient iNKT cells
↓ Cellular Survival
↓ Cytokine Secretion

Figure 6

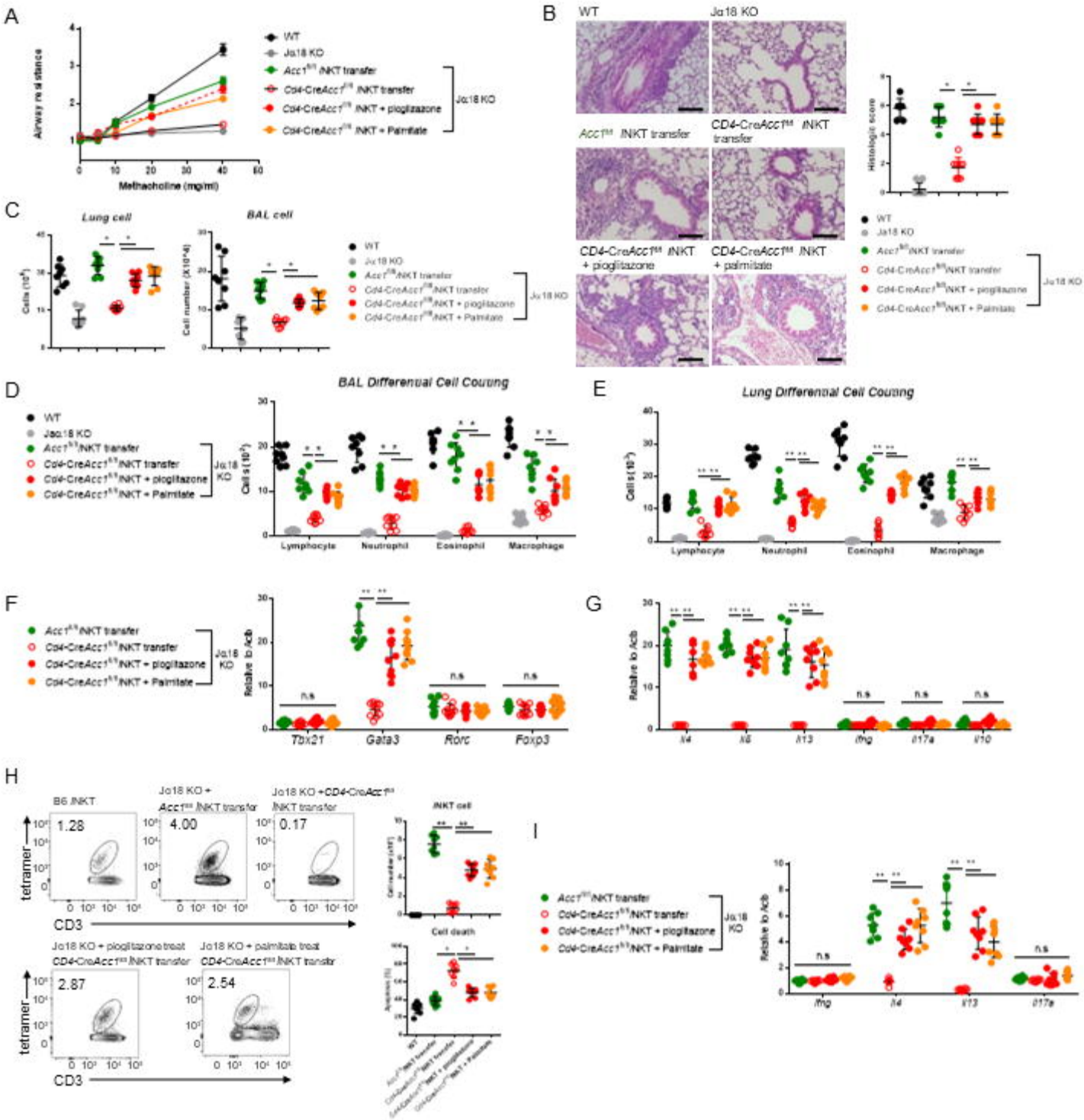
A
Airway resistance
Methacholine (mg/ml)
WT
Jα18 KO
Acc1fl/fl iNKT transfer
Cd4-CreAcc1fl/fl iNKT transfer
Cd4-CreAcc1fl/fl iNKT + pioglitazone
Cd4-CreAcc1fl/fl iNKT + Palmitate
Jα18 KO
B
WT
Jα18 KO
Acc1fl/fl iNKT transfer
CD4-CreAcc1fl/fl iNKT transfer
CD4-CreAcc1fl/fl iNKT + pioglitazone
CD4-CreAcc1fl/fl iNKT + palmitate
Histologic score
C
Lung cell
BAL cell
Cell number (X10^4)
D
BAL Differential Cell Counting
Cells (10^3)
Lymphocyte
Neutrophil
Eosinophil
Macrophage
E
Lung Differential Cell Counting
F
Relative to Actb
Tbx21
Gata3
Rorc
Foxp3
n.s
G
Il4
Il6
Il13
Ifng
Il17a
Il10
H
B6 iNKT
Jα18 KO + Acc1fl/fl iNKT transfer
Jα18 KO +CD4-CreAcc1fl/fl iNKT transfer
1.28
4.00
0.17
tetramer
CD3
Jα18 KO + pioglitazone treat CD4-CreAcc1fl/fl iNKT transfer
Jα18 KO + palmitate treat CD4-CreAcc1fl/fl iNKT transfer
2.87
2.54
iNKT cell
Cell death
I
Ifng
Il4
Il13
Il17a
J
PPARγ
2-NBDG
GLUT1
CD4-CreAcc1fl/fl iNKT + palmitate
CD4-CreAcc1fl/fl iNKT +pioglitazone
CD4-CreAcc1fl/fl iNKT
Acc1fl/fl iNKT
Control
MFI

Figure S1

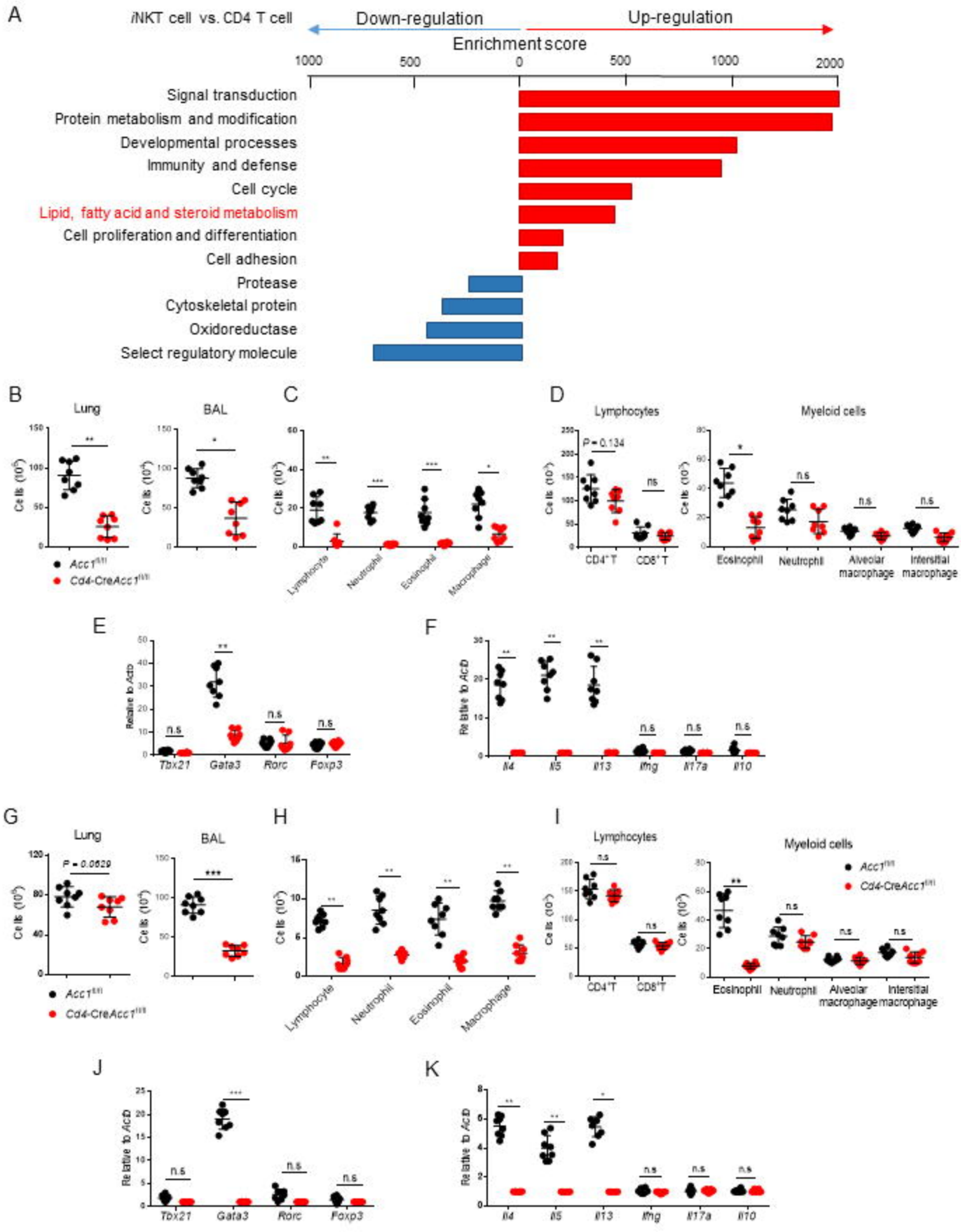
A
iNKT cell vs. CD4 T cell
Down-regulation
Up-regulation
Enrichment score
1000
500
0
500
1000
2000
Signal transduction
Protein metabolism and modification
Developmental processes
Immunity and defense
Cell cycle
Lipid, fatty acid and steroid metabolism
Cell proliferation and differentiation
Cell adhesion
Protease
Cytoskeletal protein
Oxidoreductase
Select regulatory molecule
B
Lung
BAL
C
D
Lymphocytes
Myeloid cells
P = 0.134
ns
n.s
CD4+ T
CD8+ T
Eosinophil
Neutrophil
Alveolar macrophage
Interstitial macrophage
Lymphocyte
Macrophage
Acc1fl/fl
Cd4-CreAcc1fl/fl
E
F
Tbx21
Gata3
Rorc
Foxp3
Il4
Il5
Il13
Ifng
Il17a
Il10
G
P = 0.0629
H
I
J
K

Figure S2

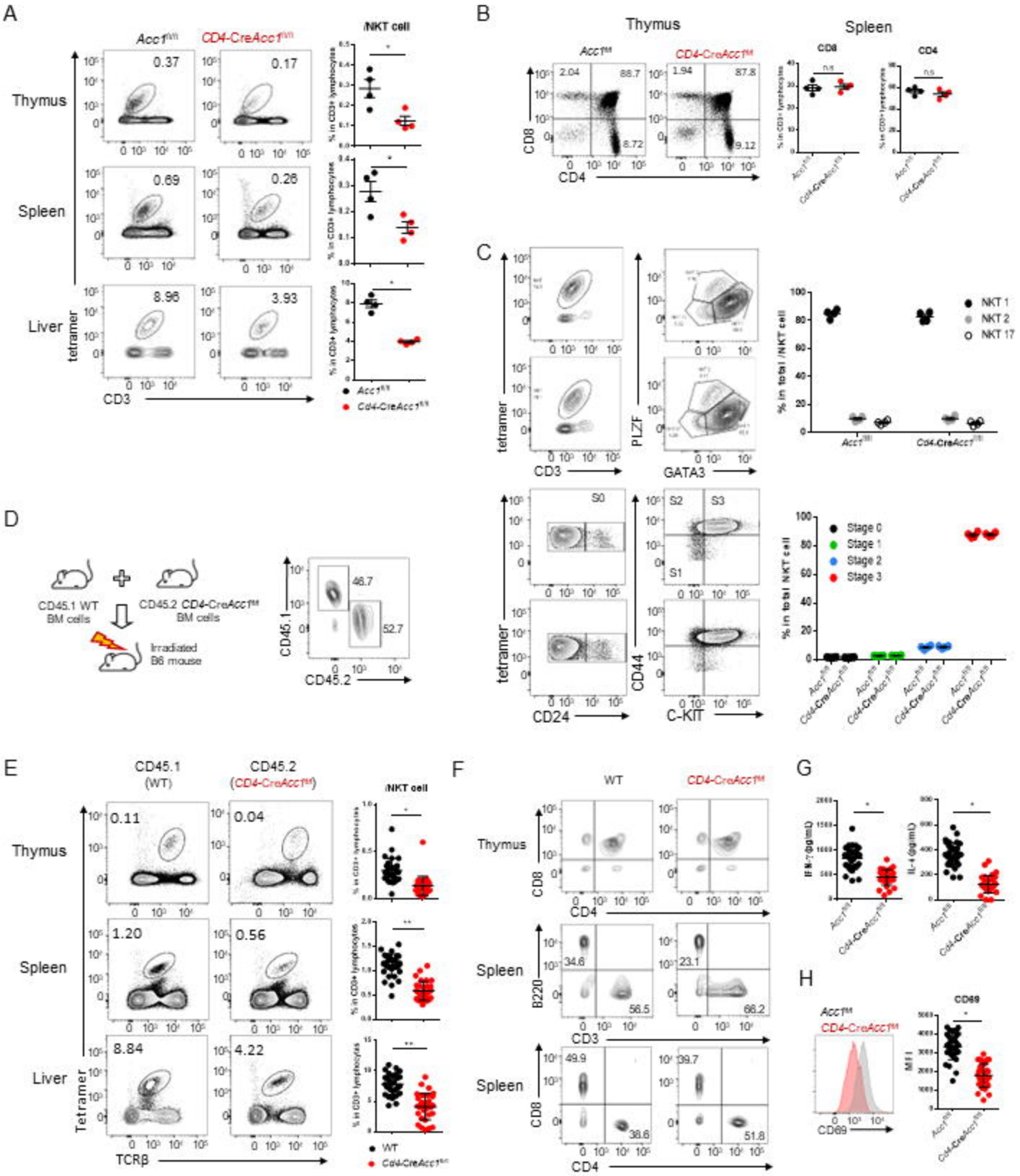
A
Acc1fl/fl
CD4-CreAcc1fl/fl
iNKT cell
Thymus
Spleen
Liver
tetramer
CD3
0.37
0.17
0.69
0.26
8.96
3.93
% in CD3+ lymphocytes
B
Thymus
Spleen
CD8
CD4
2.04
88.7
8.72
1.94
87.8
9.12
n.s
C
tetramer
CD3
PLZF
GATA3
NKT 1
NKT 2
NKT 17
% in total iNKT cell
S0
S1
S2
S3
CD24
CD44
C-KIT
Stage 0
Stage 1
Stage 2
Stage 3
D
CD45.1 WT BM cells
CD45.2 CD4-CreAcc1fl/fl BM cells
Irradiated B6 mouse
CD45.1
CD45.2
46.7
52.7
E
CD45.1 (WT)
CD45.2 (CD4-CreAcc1fl/fl)
iNKT cell
Thymus
Spleen
Liver
Tetramer
TCRβ
0.11
0.04
1.20
0.56
8.84
4.22
% in CD3+ lymphocytes
WT
Cd4-CreAcc1fl/fl
F
WT
CD4-CreAcc1fl/fl
Thymus
Spleen
CD8
CD4
B220
CD3
34.6
56.5
23.1
66.2
49.9
38.6
39.7
51.8
G
IFN-γ (pg/mL)
IL-4 (pg/mL)
H
Acc1fl/fl
CD4-CreAcc1fl/fl
CD69
MFI

Figure S3

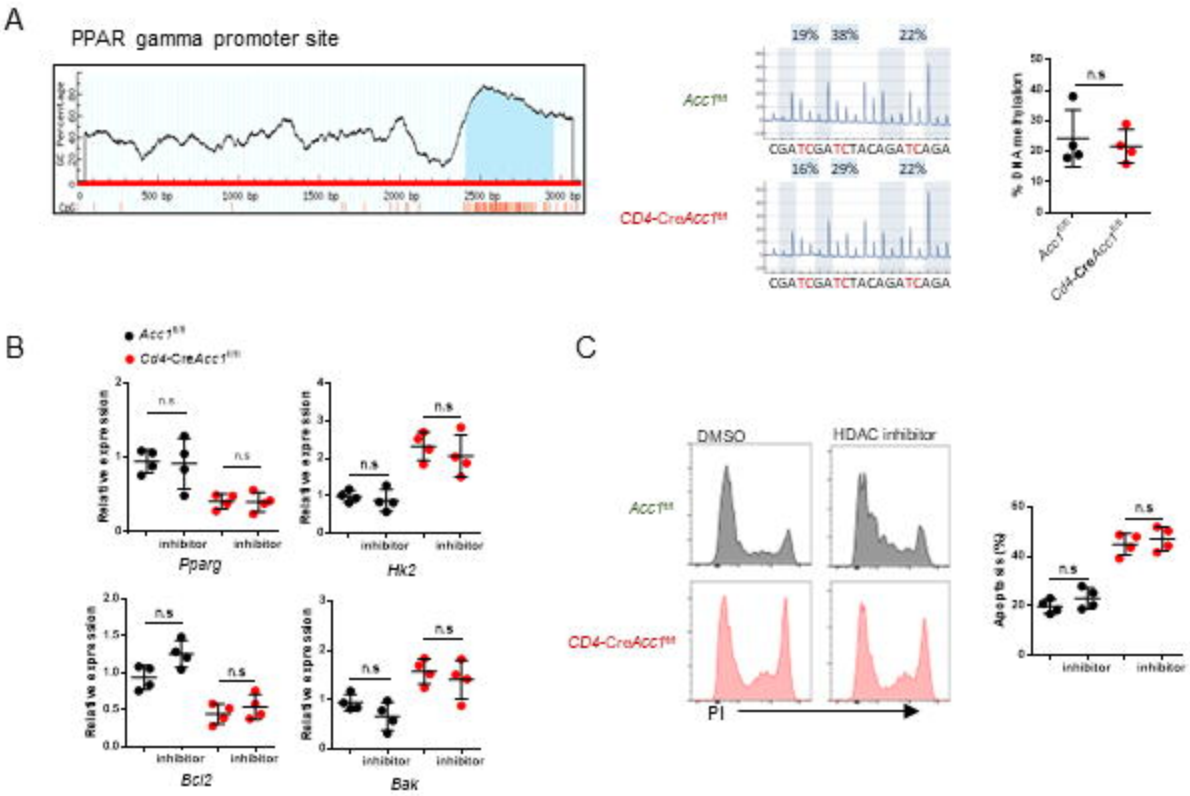
A
PPAR gamma promoter site
500 bp
1000 bp
1500 bp
2000 bp
2500 bp
3000 bp
19%
38%
22%
Acc1fl/fl
CGATCGATCTACAGATCAGA
16%
29%
22%
CD4-CreAcc1fl/fl
CGATCGATCTACAGATCAGA
n.s
% DNA methylation
Acc1fl/fl
CD4-CreAcc1fl/fl
B
Acc1fl/fl
Cd4-CreAcc1fl/fl
Relative expression
n.s
inhibitor
Pparg
Hk2
Bcl2
Bak
C
DMSO
HDAC inhibitor
Acc1fl/fl
CD4-CreAcc1fl/fl
PI
Apoptosis (%)

Figure S4

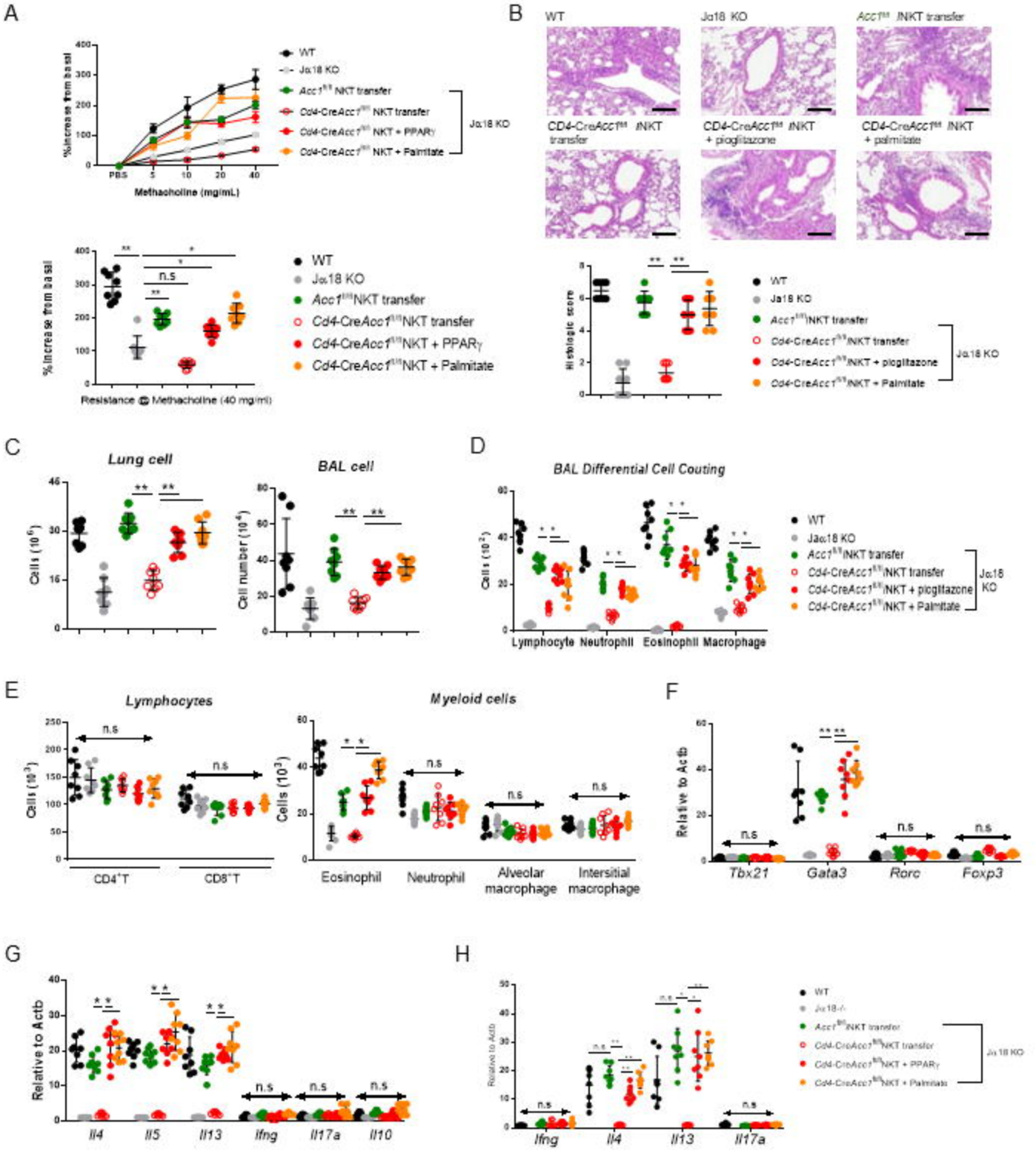
A
B
C
D
E
F
G
H
WT
Jα18 KO
Acc1fl/fl NKT transfer
Cd4-CreAcc1fl/fl NKT transfer
Cd4-CreAcc1fl/fl NKT + PPARγ
Cd4-CreAcc1fl/fl NKT + Palmitate
Jα18 KO
% increase from basal
Methacholine (mg/mL)
Resistance @ Methacholine (40 mg/ml)
CD4-CreAcc1fl/fl iNKT transfer
CD4-CreAcc1fl/fl iNKT + pioglitazone
CD4-CreAcc1fl/fl iNKT + palmitate
Histologic score
Lung cell
BAL cell
Cell number (10⁴)
BAL Differential Cell Couting
Lymphocyte
Neutrophil
Eosinophil
Macrophage
Lymphocytes
Myeloid cells
CD4⁺T
CD8⁺T
Alveolar macrophage
Intersitial macrophage
Relative to Actb
Tbx21
Gata3
Rorc
Foxp3
Il4
Il5
Il13
Ifng
Il17a
Il10
n.s

Figure S5

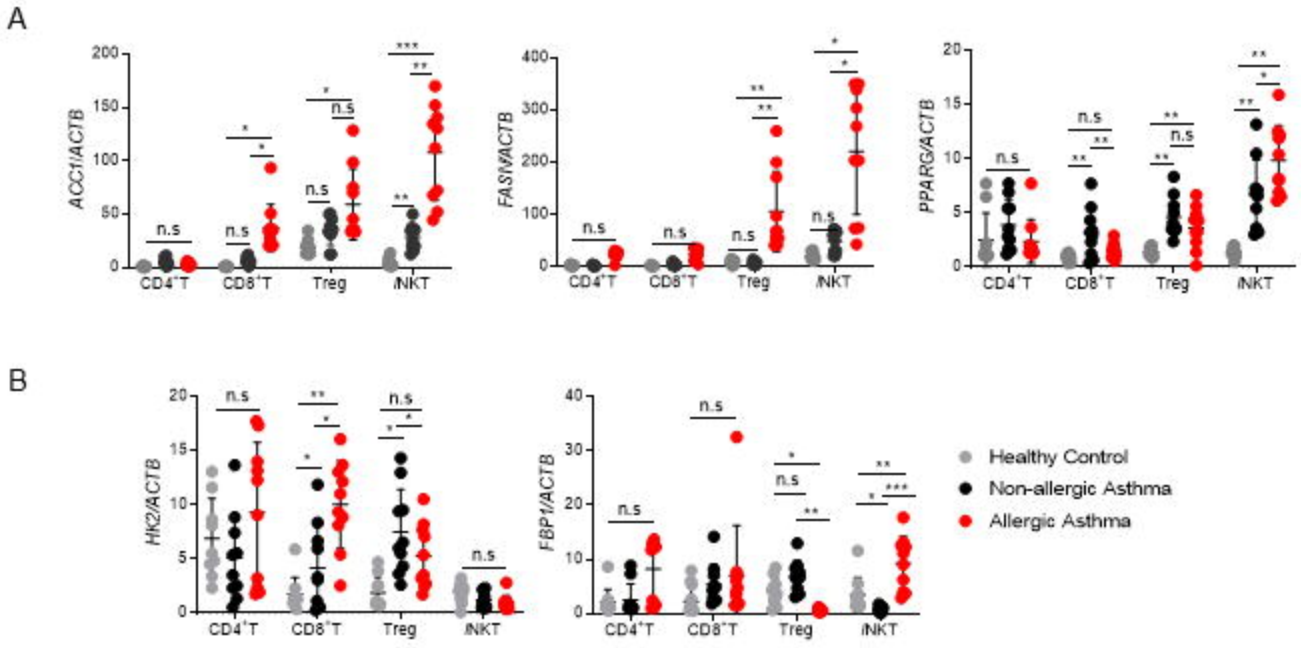
A
ACC1/ACTB
FASN/ACTB
PPARG/ACTB
CD4+T
CD8+T
Treg
iNKT
n.s
B
HK2/ACTB
FBP1/ACTB
Healthy Control
Non-allergic Asthma
Allergic Asthma